DIMENSION REDUCED ROBUST BEAMFORMING FOR TOWED ARRAYS

A THESIS SUBMITTED TO
THE GRADUATE SCHOOL OF NATURAL AND APPLIED SCIENCES
OF
MIDDLE EAST TECHNICAL UNIVERSITY

BY

EMRE TOPÇU

IN PARTIAL FULFILLMENT OF THE REQUIREMENTS
FOR
THE DEGREE OF MASTER OF SCIENCE
IN
ELECTRICAL AND ELECTRONICS ENGINEERING

SEPTEMBER 2015

Approval of the thesis:

DIMENSION REDUCED ROBUST BEAMFORMING FOR TOWED ARRAYS

submitted by **EMRE TOPÇU** in partial fulfillment of the requirements for the degree of **Master of Science in Electrical and Electronics Engineering Department, Middle East Technical University** by,

Prof. Dr. Gülbin Dural Ünver _____
Dean, Graduate School of **Natural and Applied Sciences**

Prof. Dr. Gönül Turhan Sayan _____
Head of Department, **Electrical and Electronics Engineering**

Prof. Dr. Çağatay Candan _____
Supervisor, **Electrical and Electronics Eng. Dept., METU**

Examining Committee Members:

Prof. Dr. Tolga Çiloğlu
Electrical and Electronics Engineering Dept., METU _____

Prof. Dr. Çağatay Candan
Electrical and Electronics Engineering Dept., METU _____

Assoc. Prof. Dr. Umut Orguner
Electrical and Electronics Engineering Dept., METU _____

Assoc. Prof. Dr. Ali Cafer Gürbüz
Electrical and Electronics Engineering Dept., TOBB ETU _____

Assist. Prof. Dr. Elif Vural
Electrical and Electronics Engineering Dept., METU _____

Date: _____

I hereby declare that all information in this document has been obtained and presented in accordance with academic rules and ethical conduct. I also declare that, as required by these rules and conduct, I have fully cited and referenced all material and results that are not original to this work.

Name, Last Name: EMRE TOPÇU

Signature :

ABSTRACT

DIMENSION REDUCED ROBUST BEAMFORMING FOR TOWED ARRAYS

Topçu, Emre

M.S., Department of Electrical and Electronics Engineering

Supervisor : Prof. Dr. Çağatay Candan

September 2015, 59 pages

Adaptive beamforming methods are used to obtain higher signal to interference plus noise ratio at the array output. However, these methods are very sensitive to steering vector and covariance matrix estimation errors. To overcome this issue, robust methods are usually employed. On the other hand, implementation of these robust methods can be computationally expensive for arrays with large number of sensors. Reduced dimension techniques aim to lower the computational load of adaptive beamforming algorithms with a minor loss of performance.

In this thesis, the reduced dimension method is combined with the robust adaptive beamforming technique in order to obtain a rapidly converging, low complexity beamformer which is robust against the steering vector mismatches and small number of training snapshots. Moreover, a dimension reduction matrix that suppresses the known interferences such as the main-ship noise for towed

arrays is designed to enhance the performance of the reduced dimension beamformer. The performance of the developed technique is illustrated by using both the simulated data (generated for different types of steering vector mismatches) and the field data obtained by a towed array in actual sea trials.

Keywords: Dimension Reduction, Robust Beamforming, Towed Array, The Dimension Reducing Matrix, Worst Case Performance Optimization

ÖZ

ÇEKİLİ DİZİNLER İÇİN DÜŞÜK BOYUTA İNDİRGENMİŞ GÜRBÜZ IŞIN DEMETLEME

Topçu, Emre
Yüksek Lisans, Elektrik Elektronik Mühendisliği Bölümü
Tez Yöneticisi : Prof. Dr. Çağatay Candan

Eylül 2015 , 59 sayfa

Uyarlamalı ışın demetleme yöntemleri, dizin çıktısında daha yüksek sinyal parazit artı gürültü oranı elde etmek için kullanılırlar. Fakat bu yöntemler yönlendirme vektörü ve kovaryans matrisi hatalarına çok hassastırlar. Bu sorunu çözmek için genellikle gürbüz yöntemler kullanılmaktadır. Ancak, gürbüz yöntemlerin gerçekleştirilmesi, yüksek sayıda sensöre sahip olan dizinler için hesaplama yükü açısından pahalıdır. Düşük boyuta indirgenmiş yöntemler ise, uyarlamalı ışın demetleme yöntemlerinde kontrollü bir biçimde performanstan feragat ederek işlem yükünü düşürmeyi amaçlar.

Bu tez kapsamında, boyut indirgeme yöntemi, gürbüz ışın demetleme tekniği ile birleştirilerek, hızlı bir şekilde yakınsayan, yönlendirme vektörü uyumsuzluğuna ve düşük sayıdaki eğitim verisinden kaynaklanan hatalara karşı gürbüz, düşük işlem yükü getiren bir ışın demetleme yöntemi elde etmek amaçlanmaktadır. Boyut indirgenmiş ışın demetleme yönteminin performansını arttırmak için bi-

linen parazitleri (örneğin çekili dizinler için ana gemi gürültüsünü) bastıran bir boyut indirgeme matrisi tasarlanmıştır. Geliştirilen yöntemin performansı benzetim verileri (farklı yönlendirme vektörü hataları için) ve deniz testlerinde çekili dizinle elde edilen gerçek veriler kullanılarak test edilmiştir.

Anahtar Kelimeler: Boyut İndirgeme, Gürbüz Işın Demetleme, Çekili Dizin, Boyut İndirgeme Matrisi, En Kötü Durum için Performans Optimizasyonu

To my family

ACKNOWLEDGMENTS

I would like to express the deepest appreciation to Prof. Dr. Çağatay Candan for his support, understanding and guidance throughout the development of this thesis study. Without his supervision, patience and encouragement, this thesis would not have been completed.

I thank TÜBİTAK for its support throughout this thesis. I would also like to thank ASELSAN Inc. for the support and encouragement on academic studies.

I really appreciate the support of my friends, who “hopefully" never resented me when I rejected their plans to hang out as I needed to “work on my thesis". With their love and understanding I managed to overcome the difficulties in the process.

Finally, I would like to express my special thanks to my parents for their love, trust, understanding and every kind of support not only throughout my thesis but also throughout my life.

TABLE OF CONTENTS

LIST OF TABLES

TABLES

LIST OF FIGURES

FIGURES

LIST OF ABBREVIATIONS

BTR	Bearing Time Record
DOA	Direction of Arrival
INR	Interference to Noise Ratio
LCMV	Linearly Constrainted Minimum Variance
MVDR	Minimum Variance Distortionless Response
RCB	Robust Capon Beamforming
SINR	Signal to Interference-plus-Noise Ratio
SMI	Sample Matrix Inversion
SOI	Signal of Interest
SNR	Signal to Noise Ratio
ULA	Uniform Linear Array

CHAPTER 1

INTRODUCTION

1.1 Introduction

Beamforming or spatial filtering is a signal processing technique often used for extracting information from signals obtained by an array of sensors and has been widely used in numerous applications such as radar, sonar, wireless communications, microphone arrays, seismology, medical imaging, and other areas. The main objective of beamforming is to estimate the direction of desired signals in the presence of noise and interference.

Beamformers can be categorized as either data independent or data dependent. Data independent beamformers use the preestablished beamformer coefficients to provide the distortionless response in the desired signal directions [27]. The major disadvantage of the data independent beamformers is that these methods do not have interference rejection capability. On the other hand, the data dependent beamformers (sometimes referred as adaptive beamformers) optimize the beamformer coefficients, using second order statistics of operational environment, to maximally suppress interference and noise while maintaining a distortionless response at the desired direction. The adaptive beamformer coefficients have to be regularly updated based on the collected statistics from the array output.

The adaptive beamformers can provide an increased signal to interference plus noise ratio (SINR) at the array output compared to the data independent beamformers, thanks to the interference rejection capability. They have higher resolu-

tion than the data independent methods. However, the performance of adaptive beamformers can substantially degrade if the array response to the desired signal is not known exactly [6, 28, 29].

In practical applications, discrepancies may occur between the assumed steering vector and the true steering vector as a consequence of look direction mismatch [18], array imperfections [17], environment inhomogeneities [22], near-field problem [15], local scattering [1] and some other effects. Adaptive beamformers are especially sensitive to steering vector mismatches. In the presence of such a mismatch, adaptive beamformers tend to suppress the incoming desired signal treating it as an interference, instead of maintaining the distortionless response at the look direction [16]. Consequently, robust and adaptive approaches are required in many practical applications.

Several methods providing robustness against steering vector mismatches have been developed in the literature. The most common method called as the Linearly Constrained Minimum Variance (LCMV) beamformer is presented in [10] and [25]. Also in [3], a robust beamforming method is derived via a Bayesian approach. These methods are robust only to uncertainties in the steering vector caused by the signal look direction mismatches. Several other methods such as the quadratically constrained beamformer [7] and the eigenspace-based beamformer [5,9] are able to partly overcome the arbitrary steering vector mismatches as well. The quadratically constrained beamformer is based on the diagonal loading of the sample covariance matrix and it is in general not clear how to obtain the diagonal loading factor. The eigenspace-based beamformer is ineffective at low Signal to Noise Ratios (SNR) since it is very sensitive to the knowledge of signal plus interference subspace.

In [11], a robust adaptive method in the presence of the unknown steering vector mismatches is presented. This method is based on the worst case performance optimization. This beamformer can also be interpreted as a diagonal loading approach, however for this method, it is sufficient to have an upper bound of diagonal loading, which is typically calculated using the norm of the steering vector mismatch.

In practice, another cause of performance degradation of adaptive beamformers is the small number of available training snapshots caused by the nonstationarity of the environment, array position and shape and moving sources. It is well known that the number of the stationary training snapshots that are used to estimate the sample covariance matrix should be at least two times higher than the number of elements in the array [21]. To overcome this problem, several methods have been developed. Most popular of them is diagonal loading [4, 7]. Another technique that increases the effective number of training snapshots is the null-broadening in the direction of the moving interferers as given in [24]. Although this method is effective against the snapshot deficiency, its computational complexity for arrays with a large number of elements is high.

For arrays with a large number of elements, the dimension reduction technique can be used to obtain rapidly converging, low complexity beamformers. After projecting the array output to a reduced dimension subspace by using a dimension reducing transform, robustness against the steering vector mismatches can be provided by performing the robust methods within this subspace. Moreover, dimension reduction decreases the performance degradation of the robust and adaptive methods that is induced by the small number of training snapshots. However, dimension reduction results in less degrees of freedom (the number of unconstrained of free weights). Consequently, there is a trade off between choosing a dimension small enough to have the desired algorithm convergence and high enough to provide sufficient degrees of freedom.

In the literature, several dimension reduction methods have been developed. These methods can be separated as data independent (such as beamspace [12,27], subarray processing [8]) and data dependent [13, 14]. Although the data dependent dimension reduction methods have better rejection capabilities against out of sector sources, they are in general computationally expensive for real-time operations.

In [23], the reduced dimension method [12] is combined with the Robust Capon Beamforming [19, 25, 26]. However, a dimension reduced subspace is not described. The performance of the developed method is examined only for a sub-

space that is comprised of a set of conventional beams.

1.2 Scope of the Thesis

The aim of this work is to combine the reduced dimension method given in [23] and the robust adaptive beamforming technique in [11] in order to have a rapidly converging, reduced dimension beamformer that is robust against the steering vector mismatches and small number of training snapshots. Moreover, the dimension reducing matrix that suppresses the known interferences such as main-ship noise for towed arrays is designed to enhance the performance of the reduced dimension beamformer.

The performance of the beamformer techniques described in Chapter 2 are examined by using both the simulated data (generated for different types of steering vector mismatch) and the real data (obtained by the towed array of ASELSAN in sea trials).

1.3 Outline

In Chapter 2, the signal model used in all simulations and some background of adaptive beamforming are presented. Then the robust adaptive beamformer, Worst Case Performance Optimization, is reviewed. In Section 2.6, the combination of the reduced dimension method and the worst case performance optimization beamformer is illustrated and in Subsection 2.6.1, the dimension reducing matrix design is described.

Chapter 3 presents the simulation and experimental results where the performance of the reduced dimension robust adaptive beamformer with the designed subspace is compared with the methods described in Chapter 2.

Chapter 4 contains concluding remarks.

CHAPTER 2

BEAMFORMING TECHNIQUES

In this chapter, first the signal model used throughout this work is given. Then, some beamforming techniques and a robust-adaptive reduced dimension method are described.

2.1 Signal Model

The standard narrowband beamforming model is used in this study. In this model, it is assumed that K narrowband plane wave signals are impinging on an array of M sensors, where $K < M$. The array output is modeled as

$$\begin{aligned} \mathbf{y}(t) &= \mathbf{a}(\phi_0)s(t) + \sum_{k=1}^{K-1} \mathbf{a}(\phi_k)s_k(t) + \mathbf{n}(t) \\ &= \mathbf{a}(\phi_0)s(t) + \mathbf{i}(t) + \mathbf{n}(t) \\ &= \mathbf{a}(\phi_0)s(t) + \mathbf{e}(t) \end{aligned} \tag{2.1}$$

where $\mathbf{y}(t) = [y_0(t)\ y_1(t)\ \cdots\ y_{M-1}(t)]^T \in \mathbb{C}_{M\times 1}$ is the array output, M is the number of sensors, $\mathbf{a}(\phi)$ is the steering vector (also named as the manifold vector), $s(t)$, $\mathbf{i}(t)$, $\mathbf{n}(t)$ are the signal of interest (SOI), $K-1$ interfering sources and noise, respectively.

The elements of the steering vector consists of the exponential function whose exponent is related with the phase delays between reference sensor and the remaining sensors of the array. The steering vector for the signal impinging on

the array from the azimuth angle ϕ_0 can be defined as

$$\mathbf{a}(\phi_0) = [e^{-j\frac{2\pi}{\lambda}(P_{x_0}\cos(\phi_0)+P_{y_0}\sin(\phi_0))} \ \cdots \ e^{-j\frac{2\pi}{\lambda}(P_{x_{M-1}}\cos(\phi_0)+P_{y_{M-1}}\sin(\phi_0))}]^T \quad (2.2)$$

where λ is the wavelength, P_{x_i}, P_{y_i} are the xy positions of i^{th} sensor, respectively and $(.)^T$ stands for the transpose. Sensor positions of Uniform Linear Array (ULA) can be written as

$$\begin{aligned} \mathbf{P}_x &= [0 \quad d \quad 2d \quad \cdots \quad (M-1)d], \\ \mathbf{P}_y &= [0 \quad 0 \quad 0 \quad \cdots \quad 0]. \end{aligned} \quad (2.3)$$

Using (2.3), the steering vector for the ULA becomes

$$\mathbf{a}(\phi_0) = [1 \ e^{-j\frac{2\pi}{\lambda}d\cos(\phi_0)} \ e^{-j\frac{2\pi}{\lambda}2d\cos(\phi_0)} \ \cdots \ e^{-j\frac{2\pi}{\lambda}(M-1)d\cos(\phi_0)}]^T. \quad (2.4)$$

Following the general convention, we do not normalize the steering vector and we have

$$\|\mathbf{a}(\phi_0)\|^2 = M. \quad (2.5)$$

The narrowband beamformer output is given by

$$\begin{aligned} y_F(t) &= \mathbf{w}^H\mathbf{y}(t) \\ &= \mathbf{w}^H\mathbf{a}(\phi_0)s(t) + \mathbf{w}^H\mathbf{e}(t) \end{aligned} \quad (2.6)$$

where $\mathbf{w} \in \mathbb{C}_{M\times 1}$ is the beamformer coefficients and $(.)^H$ stands for the Hermitian transpose. The signal to interference plus noise ratio (SINR) at the beamformer output can be found by using (2.6)

$$\text{SINR} = \frac{\mathbf{w}^H\mathbf{R}_s\mathbf{w}}{\mathbf{w}^H\mathbf{R}_e\mathbf{w}}. \quad (2.7)$$

Here $\mathbf{R}_s$ is the covariance matrix of SOI and $\mathbf{R}_e$ is the covariance matrix of interference plus noise,

$$\begin{aligned} \mathbf{R}_s &= \text{E}[(\mathbf{a}(\phi_0)s(t))(\mathbf{a}(\phi_0)s(t))^H] \\ &= \sigma_s^2\mathbf{a}(\phi_0)\mathbf{a}(\phi_0)^H \\ \mathbf{R}_e &= \text{E}[\mathbf{e}(t)\mathbf{e}(t)^H], \end{aligned} \quad (2.8)$$

and $\sigma_s^2 = \text{E}[|s(t)|^2]$ is the power of SOI. Inserting (2.8) into (2.7), SINR can be written as

$$\text{SINR} = \frac{\sigma_s^2|\mathbf{w}^H\mathbf{a}(\phi_0)|^2}{\mathbf{w}^H\mathbf{R}_e\mathbf{w}}. \quad (2.9)$$

2.2 Conventional Beamformer

Conventional beamformer is a data independent beamformer and also called as delay and sum beamformer. The main goal of this method is to emphasize signals coming from a certain direction and minimize beamformer output with the white noise and no interference assumptions. In order to achieve this, phase shifts are applied to each sensor output by using preset beamformer coefficients. By doing so, the array can be steered to a desired direction.

Then, desired response can be written as

$$\mathbf{w}^H \mathbf{a}(\phi_0) = 1. \tag{2.10}$$

Using (2.8) and (2.10) together with diffuse noise and no interference assumptions, the beamformer coefficients can be found easily as

$$\mathbf{w} = \frac{\mathbf{a}(\phi_0)}{M}. \tag{2.11}$$

Although conventional beamformer is simple and has low computation complexity, it does not guarantee robustness against steering vector mismatches, sensor placement errors, calibration errors, etc. Therefore, these mismatches and errors may cause a degradation of performance. Moreover, conventional beamformer cannot adapt null responses for interference rejection since beamformer coefficients are calculated without using array data and statistics.

2.3 Minimum Variance Distortionless Response (MVDR) Beamformer

Minimum variance distortionless response beamformer (MVDR) is designed using the statistics of the array output. The main goal is to optimize the beamformer coefficients such that the beamformer output contains minimal contributions from interferences and noise while maintaining a distortionless response for the SOI. That is, the beamformer coefficients can be obtained by maximizing the SINR (2.9)

$$\min_{\mathbf{w}} \mathbf{w}^H \mathbf{R}_e \mathbf{w} \quad s.t \quad \mathbf{w}^H \mathbf{a}(\phi_0) = 1. \tag{2.12}$$

The optimization problem given in (2.12) has well known analytical solution [25], which is given as

$$\mathbf{w} = \frac{\mathbf{R}_e^{-1}\mathbf{a}(\phi_0)}{\mathbf{a}(\phi_0)^H\mathbf{R}_e^{-1}\mathbf{a}(\phi_0)}. \tag{2.13}$$

The expression (2.13) gives the optimal beamformer coefficients under the assumption that the steering vector and $\mathbf{R}_e$ are exactly known in the case of a point source. However, MVDR cannot be used in practical applications since exact covariance matrix $\mathbf{R}_e$ is unavailable. There are some additional technicalities on the utilization of the MVDR beamformer. These will be explained next.

2.4 Sample Matrix Inversion (SMI) Beamformer

In practical applications, the covariance matrix of interference-plus-noise $\mathbf{R}_e$ is unavailable. A common method is to use the sample covariance matrix given in (2.14)

$$\hat{\mathbf{R}} = \frac{1}{N}\sum_{n=1}^{N}\mathbf{y}(n)\mathbf{y}(n)^H. \tag{2.14}$$

Here N is the number of training snapshots. In this case, the optimization problem in (2.12) can be rewritten as

$$\min_{\mathbf{w}} \mathbf{w}^H\hat{\mathbf{R}}\mathbf{w} \quad s.t \quad \mathbf{w}^H\mathbf{a}(\phi_0) = 1. \tag{2.15}$$

The solution to the problem (2.15) is given by [25]

$$\mathbf{w} = \frac{\hat{\mathbf{R}}^{-1}\mathbf{a}(\phi_0)}{\mathbf{a}(\phi_0)^H\hat{\mathbf{R}}^{-1}\mathbf{a}(\phi_0)}. \tag{2.16}$$

The solution of this modified problem is usually referred to as Sample Matrix Inversion (SMI) beamformer. The use of the sample covariance matrix (2.14) instead of the exact covariance matrix of interference-plus-noise (2.8) causes a certain performance degradation when the training snapshots contain SOI components. Under the assumption that the SOI component is not present in the training data, the SINR of SMI beamformer output converges to the

optimum SINR

$$\text{SINR}_{opt} = \sigma_s^2 \mathbf{a}(\phi_0)^H \mathbf{R}_e^{-1} \mathbf{a}(\phi_0). \tag{2.17}$$

It is well known that if *the signal-free training data is available*, the performance loss of SMI beamformer is less than 3 dB on average, relative to (2.17) if the following condition is satisfied [21]

$$N \geq M. \tag{2.18}$$

However, this rule is no longer valid if the training data is contaminated with the SOI. In such cases, the convergence of the SMI beamformer to (2.17) is much slower. Consequently, the SMI beamformer requires $N \gg M$ in practical applications. Figure 2.1 shows the performance of the SMI beamformer with respect to the SINR versus number of training snapshots in the ideal case (no mismatch and steering vector is exactly known). In this example, SOI is impinging from $\theta_s = 90^\circ$ (broadside) on a ULA that has $M = 32$ omnidirectional sensors spaced half a wavelength apart and Signal to Noise Ratio (SNR) is -10 dB. There are 2 interfering sources with the directions of arrival (DOAs) 30° and 50°, respectively and Interference to Noise Ratio (INR) of each interfering source is 30 dB. Note that even in this ideal case, the performance of the SMI beamformer drastically decreases with decreasing number of training snapshots.

In practice, there may be a certain level of mismatch between the assumed and actual steering vector and the SMI beamformer does not provide sufficient robustness against this steering vector mismatch. In case of steering vector mismatch, the SMI beamformer may suppress the SOI as if it was an interference and this drastically reduces the SINR at the SMI beamformer output. As an example to the steering vector mismatch, 1° look direction mismatch between the presumed and actual direction of arrival (DOA) is considered. Figure 2.2 indicates the performance of SMI in terms of bearing versus SINR for SNR $= -10$ dB and $N = 500$. This figure is generated by shifting the direction of arrival of the SOI and by calculating the SINR for each beam. As can be seen from Figure 2.2, 1° look direction mismatch leads to a substantial degradation of the output SINR.

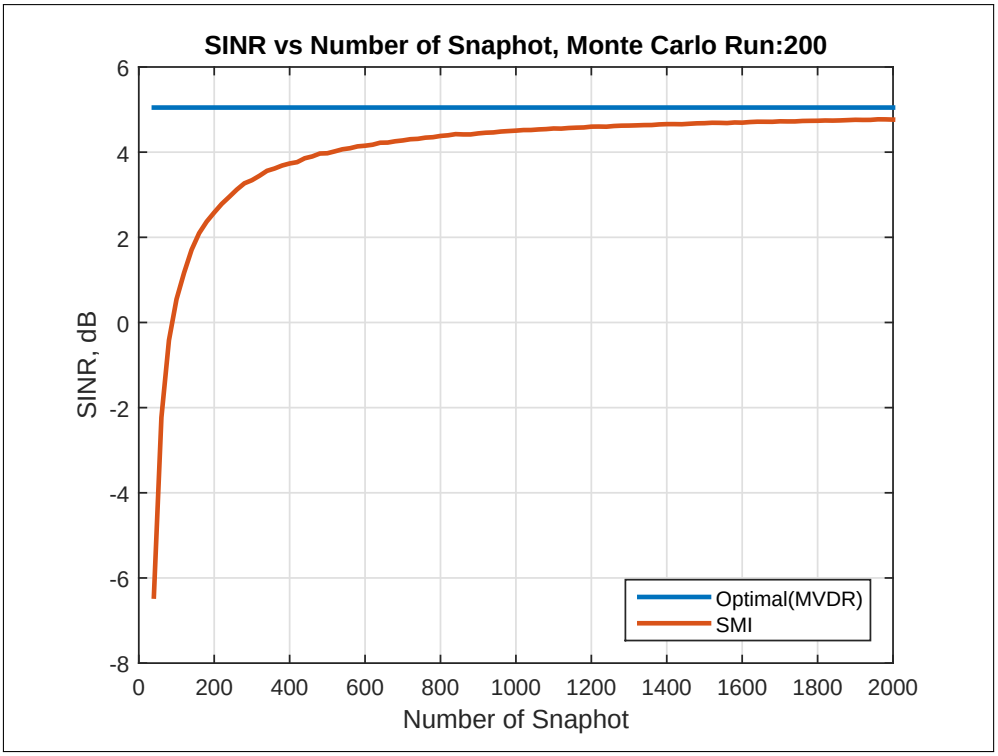

Figure 2.1: Output SINR versus number of training snapshots N, SOI: 90°, Interferences: 30° and 50°

An imperfect array calibration, unknown wavefront distortions, local scattering, nonstationarity of the environment and sources may also cause a considerable performance degradation of the SMI beamformer. Therefore, a robust adaptive beamformer is essential to improve the performance against mismatches and other errors in practical applications. This thesis aims to study robust beamforming methods which aim to provide robustness to both covariance matrix estimation errors and steering vector mismatches.

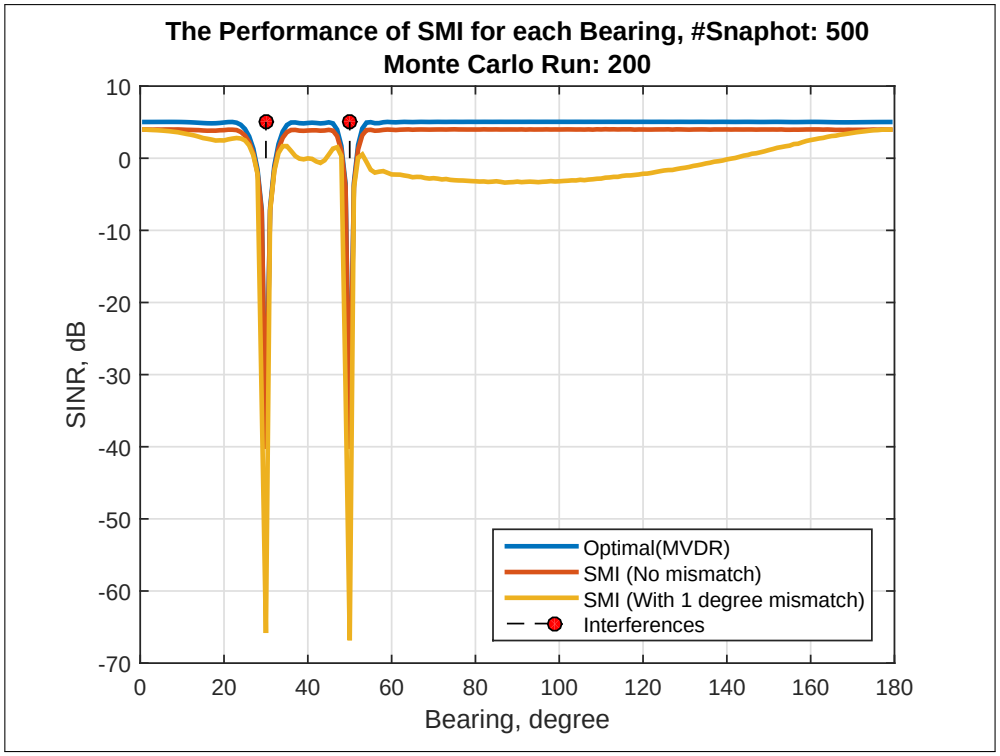

Figure 2.2: Output SINR for each bearing, $N = 500$, Interferences: 30° and 50°, SNR $= -10$

2.5 Worst-Case Performance Optimization Beamformer

In this section, the Worst-Case Performance Optimization Beamformer (WCO) [11] that is robust against the small number of training snapshots and steering vector mismatches is examined. The design principle of this beamformer is to assume the actual steering vector $\tilde{\mathbf{a}}$ as a sum of the assumed steering vector $\mathbf{a}$ and the mismatch vector δ which is a deterministic norm bounded vector. The actual steering vector is given as

$$\tilde{\mathbf{a}} = \mathbf{a} + \delta, \quad \|\delta\| \leq \epsilon \tag{2.19}$$

where ϵ is a priori known constant. Then the spherical uncertainty set can be represented as

$$\mathcal{A}(\epsilon) \triangleq \{\mathbf{c} \mid \mathbf{c} = \mathbf{a} + \delta, \quad \|\delta\| \leq \epsilon\}. \tag{2.20}$$

In order to maintain distortionless response for all possible steering vectors which belong to the spherical uncertainty set $\mathcal{A}(\epsilon)$ instead of only the assumed steering

vector $\mathbf{a}$, the SMI problem definition (2.15) is modified as

$$\min_{\mathbf{w}} \mathbf{w}^H \hat{\mathbf{R}} \mathbf{w} \quad s.t \quad |\mathbf{w}^H \mathbf{c}| \geq 1 \text{ for all } \mathbf{c} \in \mathcal{A}(\epsilon). \tag{2.21}$$

According to (2.20), the constraint of (2.21) can be rewritten as

$$\min_{\mathbf{w}} \mathbf{w}^H \hat{\mathbf{R}} \mathbf{w} \quad s.t \quad |\mathbf{w}^H (\mathbf{a} + \delta)| \geq 1 \text{ for all } \|\delta\| \leq \epsilon. \tag{2.22}$$

The constraint in (2.22) guarantees that distortionless response is maintained for all steering vectors which belong to $\mathcal{A}(\epsilon)$. That is, in the worst case, i.e. the minimum value of $|\mathbf{w}^H \mathbf{c}|$, the distortionless response can be provided with this constraint. Therefore, the robustness of beamformer against the steering vector mismatches is provided. However, (2.22) is a semi-indefinite nonconvex quadratic problem since the condition $|\mathbf{w}^H \mathbf{c}| \geq 1$ is a nonlinear and nonconvex constraint on $\mathbf{w}$ for each $\mathbf{c} \in \mathcal{A}(\epsilon)$ and it is known that this optimization problem is NP-hard and thus intractable. Surprisingly, (2.22) can be reformulated as a convex Second-Order Cone (SOC) program and then, the problem can be solved efficiently. The equivalent problem statement can be described as

$$\min_{\mathbf{w}} \mathbf{w}^H \hat{\mathbf{R}} \mathbf{w} \quad s.t \quad \min_{\delta \in D(\epsilon)} |\mathbf{w}^H \mathbf{a} + \mathbf{w}^H \delta| \geq 1 \tag{2.23}$$

where the set $D(\epsilon)$ is given by

$$\mathcal{D}(\epsilon) \triangleq \{\delta \mid \|\delta\| \leq \epsilon\}. \tag{2.24}$$

The constraint in (2.23) can be rewritten by using the triangle and Cauchy-Schwarz inequalities along with $\|\delta\| \leq \epsilon$

$$|\mathbf{w}^H \mathbf{a} + \mathbf{w}^H \delta| \geq |\mathbf{w}^H \mathbf{a}| - |\mathbf{w}^H \delta| \geq |\mathbf{w}^H \mathbf{a}| - \epsilon \|\mathbf{w}\|. \tag{2.25}$$

Moreover, if $\|\delta\| = \epsilon$ and we have $\delta = -\frac{\mathbf{w}}{\|\mathbf{w}\|} \epsilon e^{j\phi}$ where $\phi = \text{angle}\left\{\mathbf{w}^H \mathbf{a}\right\}$,

$$|\mathbf{w}^H \mathbf{a} + \mathbf{w}^H \delta| = |\mathbf{w}^H \mathbf{a}| - \epsilon \|\mathbf{w}\|. \tag{2.26}$$

Then, combining (2.25) and (2.26),

$$\min_{\delta \in D(\epsilon)} |\mathbf{w}^H \mathbf{a} + \mathbf{w}^H \delta| = |\mathbf{w}^H \mathbf{a}| - \epsilon \|\mathbf{w}\|. \tag{2.27}$$

Using (2.27), the semi-indefinite nonconvex quadratic problem (2.22) can be rewritten as a quadratic minimization problem with a single nonlinear constraint

$$\min_{\mathbf{w}} \mathbf{w}^H \hat{\mathbf{R}} \mathbf{w} \quad s.t \quad |\mathbf{w}^H \mathbf{a}| - \epsilon \|\mathbf{w}\| \geq 1. \tag{2.28}$$

The problem constraint in (2.28) is still nonconvex. However, it can be observed that the constraint is independent from the phase of $\mathbf{w}$. Therefore, the cost function can be convex by rotating the phase of $\mathbf{w}$ without affecting the objective function value. That is, $\mathbf{w}$ can be chosen such that,

$$\begin{aligned} Re\left\{\mathbf{w}^H \mathbf{a}\right\} &\geq 0, \\ Im\left\{\mathbf{w}^H \mathbf{a}\right\} &= 0. \end{aligned} \tag{2.29}$$

Using constraints (2.29) in (2.28), the convex problem formulation can be written as

$$\begin{aligned} \min_{\mathbf{w}} \mathbf{w}^H \hat{\mathbf{R}} \mathbf{w} \quad s.t \quad & \mathbf{w}^H \mathbf{a} \geq \epsilon \|\mathbf{w}\| + 1 \\ & Im\left\{\mathbf{w}^H \mathbf{a}\right\} = 0. \end{aligned} \tag{2.30}$$

The problem formulation (2.30) is now convex but it is still not suitable for CVX programming that is a Matlab-based modeling system for convex optimization. In order to develop a CVX formulation of (2.30), first step is to use the Cholesky factorization of $\hat{\mathbf{R}}$.

$$\hat{\mathbf{R}} = \mathbf{U}^H \mathbf{U}. \tag{2.31}$$

By using (2.31), the objective function of (2.30) is converted to linear function

$$\mathbf{w}^H \hat{\mathbf{R}} \mathbf{w} = \|\mathbf{U}\mathbf{w}\|^2. \tag{2.32}$$

Also inserting a new constraint and using (2.32), (2.30) can be rewritten as

$$\begin{aligned} \min_{\tau, \mathbf{w}} \tau \quad s.t \quad & \|\mathbf{U}\mathbf{w}\| \leq \tau \\ & \mathbf{w}^H \mathbf{a} \geq \epsilon \|\mathbf{w}\| + 1 \\ & Im\left\{\mathbf{w}^H \mathbf{a}\right\} = 0 \end{aligned} \tag{2.33}$$

where τ is a scalar non-negative variable. As a last step to have the CVX formulation of (2.30), (2.33) must be converted to a real-valued form. Therefore,

the new variable definitions are introduced:

$$\begin{aligned}
\breve{\mathbf{w}} &\triangleq [\, Re\{\mathbf{w}\}^T,\ Im\{\mathbf{w}\}^T\,]^T \\
\breve{\mathbf{a}} &\triangleq [\, Re\{\mathbf{a}\}^T,\ Im\{\mathbf{a}\}^T\,]^T \\
\bar{\mathbf{a}} &\triangleq [\, Im\{\mathbf{a}\}^T,\ -Re\{\mathbf{a}\}^T\,]^T \\
\breve{\mathbf{U}} &\triangleq \begin{bmatrix} Re\{\mathbf{U}\} & -Im\{\mathbf{U}\} \\ Im\{\mathbf{U}\} & Re\{\mathbf{U}\} \end{bmatrix}.
\end{aligned} \tag{2.34}$$

Using the new variable definitions in (2.34), the CVX formulation of (2.30) is obtained as

$$\begin{aligned}
\min_{\tau,\breve{\mathbf{w}}} \tau \quad s.t \quad & \|\breve{\mathbf{U}}\breve{\mathbf{w}}\| \le \tau \\
& \breve{\mathbf{w}}^H\breve{\mathbf{a}} \ge \epsilon\|\breve{\mathbf{w}}\| + 1 \\
& \breve{\mathbf{w}}^H\bar{\mathbf{a}} = 0.
\end{aligned} \tag{2.35}$$

After solving the optimization problem (2.35) in CVX, the beamformer coefficients is equal to

$$\mathbf{w}_{WCO} = [\breve{w}_1,\ \cdots\ \breve{w}_M]^T + j[\breve{w}_{M+1},\ \cdots\ \breve{w}_{2M}]. \tag{2.36}$$

As a result, the semi-indefinite nonconvex quadratic problem formulation (2.22) is converted to the canonical CVX problem formulation (2.35) and the beamformer coefficients (2.36) that are robust against the steering vector mismatch and small number of training snapshots are obtained.

2.6 Reduced Dimension Worst-Case Performance Optimization Beamformer

In this section, the Worst-Case Performance Optimization Beamformer is combined with the data independent reduced dimension technique [23] in order to decrease the computational complexity and increase the algorithm convergence for large arrays. Moreover, a subspace design to suppress the known interferences is examined. The use of this subspace for the dimension reduction enables us to use the available degrees of freedom only for the suppression of unknown interferences. Thus, the disadvantage of dimension reduction (which is the fewer degrees of freedom) is reduced.

In the data independent reduced dimension method, the M element array output $\mathbf{y} \in \mathbb{C}_{M\times 1}$ is projected onto an L dimension subspace by using a dimension reducing transformation matrix $\mathbf{D}(\phi_0) \in \mathbb{C}_{M\times L}$, where $L < M$. The reduced dimension array output can be written as

$$\mathbf{y}_{RD} = \mathbf{D}^H(\phi_0)\mathbf{y} \tag{2.37}$$

where $\mathbf{y}_{RD} \in \mathbb{C}_{L\times 1}$. And the signal model is rewritten as

$$\begin{aligned} \mathbf{y}_{RD}(t) &= \mathbf{D}^H(\phi_0)\mathbf{a}(\phi_0)s(t) + \mathbf{D}^H(\phi_0)\mathbf{e}(t) \\ &= \mathbf{b}(\phi_0)s(t) + \mathbf{e}_{RD}(t). \end{aligned} \tag{2.38}$$

The dimension reducing transformation matrix $\mathbf{D}(\phi_0)$ is often designed such that $\mathbf{D}^H(\phi_0)\mathbf{D}(\phi_0) = I_L$ so that white noise remains white after the dimension reduction.

Using (2.38), the sample covariance matrix can be calculated as

$$\begin{aligned} \hat{\mathbf{R}}_{RD} &= \frac{1}{L}\sum_{l=1}^{L} \mathbf{y}_{RD}(l)\mathbf{y}_{RD}(l)^H \\ &= \mathbf{D}^H(\phi_0)\hat{\mathbf{R}}\mathbf{D}(\phi_0). \end{aligned} \tag{2.39}$$

After projecting the array output onto the L dimensional subspace, the Worst-Case Performance Optimization Beamformer is applied to the reduced dimension array output (2.37). The problem formulation can be rewritten as

$$\min_{\bar{\mathbf{w}}} \bar{\mathbf{w}}^H\hat{\mathbf{R}}_{RD}\bar{\mathbf{w}} \quad s.t \quad |\bar{\mathbf{w}}^H\mathbf{c}| \geq 1 \text{ for all } \mathbf{c} \in \mathcal{A}_{RD}(\epsilon) \tag{2.40}$$

where $\mathcal{A}_{RD}(\epsilon) \triangleq \{\mathbf{c} \mid \mathbf{c} = \mathbf{b} + \delta, \quad \|\delta\| \leq \epsilon\}$ is a reduced dimension spherical uncertainty set, $\mathbf{b} = \mathbf{D}^H(\phi_0)\mathbf{a}$ is a reduced dimension steering vector, $\bar{\mathbf{w}} \in \mathbb{C}_{L\times 1}$ is the reduced dimension beamformer coefficient vector. The solution of this problem formulation is identical to the one given in (2.35). After solving $\bar{\mathbf{w}}$ in CVX, the beamformer coefficients can be transformed to the full-dimension

$$\mathbf{w}_{RD} = \mathbf{D}(\phi_0)\bar{\mathbf{w}}. \tag{2.41}$$

Then the beamformer output is equal to

$$y_f = \mathbf{w}_{RD}^H\mathbf{y}. \tag{2.42}$$

The computational complexity is reduced by solving the worst case optimization problem in reduced dimension. As an example, for 32 element array, the following steps must be calculated to find the beamformer coefficients

- 32x32 dimension covariance matrix must be estimated,
- The Cholesky factorization of this covariance matrix must be calculated,
- The optimization problem must be solved in 32 dimension.

If the array output is multiplied by 5x32 dimension reducing transformation matrix to get the reduced dimension array output and the beamformer coefficients are calculated in this dimension, the following steps which have lower computational complexity must be calculated.

- 5x5 dimension covariance matrix must be estimated,
- The Cholesky factorization of this covariance matrix must be calculated,
- The optimization problem must be solved in 5 dimension.

The selection of the dimension reducing transformation matrix D is crucial since dimension reduction causes the beamformer to have fewer degrees of freedom. In the next section, the dimension reducing transformation matrix is designed to suppress the known interferences such as the main ship in towed array applications.

2.6.1 Subspace Design

In this subsection, a subspace is designed to suppress the known interferences while reducing the signal dimension. Thus, the degrees of freedom decreased in consequence of dimension reduction can be used for only the unknown interferences.

In order to suppress the known interferences, a maximum tolerable loss at look direction is defined. The purpose is to provide distortionless response within

the given tolerance to the direction of the SOI while suppressing the known interferences. To ease the presentation, in this section we assume that $a(\phi)$ and w vectors are normalized so that $\|\mathbf{a}(\phi)\| = \|\mathbf{w}\| = 1$. If there is only one known interfering source from direction ϕ_1, the problem can be defined as

$$\min_{\mathbf{w}} |\mathbf{w}^H \mathbf{a}(\phi_1)| \quad s.t \quad |\mathbf{w}^H \mathbf{a}(\phi_0)| > \sqrt{1-\rho^2} \tag{2.43}$$

where $0 \leq \rho \leq 1$ is the maximum tolerable loss at a desired direction. (2.43) is a nonconvex problem since $|\mathbf{w}^H \mathbf{a}(\phi_0)| > \sqrt{1-\rho^2}$ is a nonlinear and nonconvex constraint on $\mathbf{w}$. However, (2.43) can be reformulated as a convex problem. Any vector $\mathbf{w}$ can be written as

$$\mathbf{w} = \beta \mathbf{a}(\phi_0) + \mathbf{V}\mathbf{x} \tag{2.44}$$

where $\mathbf{V} \in \mathbb{C}_{M\times(M-1)}$ is the matrix that provides the condition $\mathbf{V}^T \mathbf{a}(\phi_0) = \mathbf{0}_{M-1\times 1}$. That is, the each column of the matrix $\mathbf{V}$ is orthogonal to the vector $\mathbf{a}(\phi_0)$. $\mathbf{x} \in \mathbb{C}_{1\times(M-1)}$ is the unknown vector. By using (2.44), the constraint in (2.43) can be written as

$$|(\beta \mathbf{a}(\phi_0) + \mathbf{V}\mathbf{x})^H \mathbf{a}(\phi_0)| = |\beta| > \sqrt{1-\rho^2}. \tag{2.45}$$

Since the norm of $\mathbf{w}$ is equal to 1, the condition on β and $\mathbf{x}$ can be found as

$$\|\mathbf{w}\|^2 = |\beta|^2 + \|\mathbf{x}\|^2 = 1. \tag{2.46}$$

Combining (2.45) and (2.46),

$$\|\mathbf{x}\| < \rho. \tag{2.47}$$

The optimization problem given in (2.43) can be rewritten as

$$\min_{\mathbf{x}} |(\beta \mathbf{a}(\phi_0) + \mathbf{V}\mathbf{x})^H \mathbf{a}(\phi_1)| \quad s.t \quad \|\mathbf{x}\| < \rho. \tag{2.48}$$

The value of β in optimization problem (2.48) is not known. However, it is known that its value is between $\sqrt{1-\rho^2}$ and 1. By taking $\beta = 1$, that is selecting the maximum value for its value, the problem is relaxed to the following one:

$$\min_{\mathbf{x}} |(\mathbf{a}(\phi_0) + \mathbf{V}\mathbf{x})^H \mathbf{a}(\phi_1)| \quad s.t \quad \|\mathbf{x}\| < \rho. \tag{2.49}$$

This optimization problem is convex and can be solved by using the CVX convex optimization tool. When there are more than one interfering sources, the optimization problem can be defined as

$$\begin{aligned} \min_{\mathbf{x}} \delta \quad s.t \quad & \|\mathbf{x}\| < \rho \\ & |(\mathbf{a}(\phi_0) + \mathbf{V}\mathbf{x})^H \mathbf{a}(\phi_1)| < \delta \\ & \vdots \\ & |(\mathbf{a}(\phi_0) + \mathbf{V}\mathbf{x})^H \mathbf{a}(\phi_k)| < \delta. \end{aligned} \tag{2.50}$$

Finally, the desired steering vector is equal to

$$\mathbf{a}_d(\phi_0) = \mathbf{a}(\phi_0) + \mathbf{V}\mathbf{x}_{\text{opt}}. \tag{2.51}$$

where $\mathbf{x}_{\text{opt}}$ is the $\mathbf{x}$ vector optimized through convex programming. The desired $2L-1$ dimensional subspace with β degree intervals can be generated by using the desired steering vectors as

$$\mathbf{D}(\phi_0) = [\mathbf{a}_d(\phi_0 - L\beta) \ \cdots \ \mathbf{a}_d(\phi_0 - \beta) \ \mathbf{a}_d(\phi_0) \ \mathbf{a}_d(\phi_0 + \beta) \ \cdots \ \mathbf{a}_d(\phi_0 + L\beta)]. \tag{2.52}$$

In this study, the passive towed arrays are considered while designing the subspace. In such applications, the known interference is the noise of main ship that tows the array. Since the depth of the towed array changes with the vessel speed and there are reflections from the sea surface, the direction of the main-ship noise is assumed to be within the interval [0° 10°]. With this assumption the beams from which the desired subspace is formed are generated.

In Figure 2.3 and 2.4, conventional and designed beampatterns for different angles are compared. In Figure 2.3, it can be observed that there is a small loss in the look direction. However, the designed beam has a high suppression in the interference interval. Moreover, the loss at the look direction decreases with increasing angle difference between the desired direction and the main ship while the desired beam still has a high suppression in the interference interval. This can be seen from Figure 2.4.

As a result, the disadvantage of dimension reduction (which is the decrease in the degrees of freedom) is reduced by using the dimension reducing transformation matrix $\mathbf{D}(\phi_0)$ which only includes the designed beams.

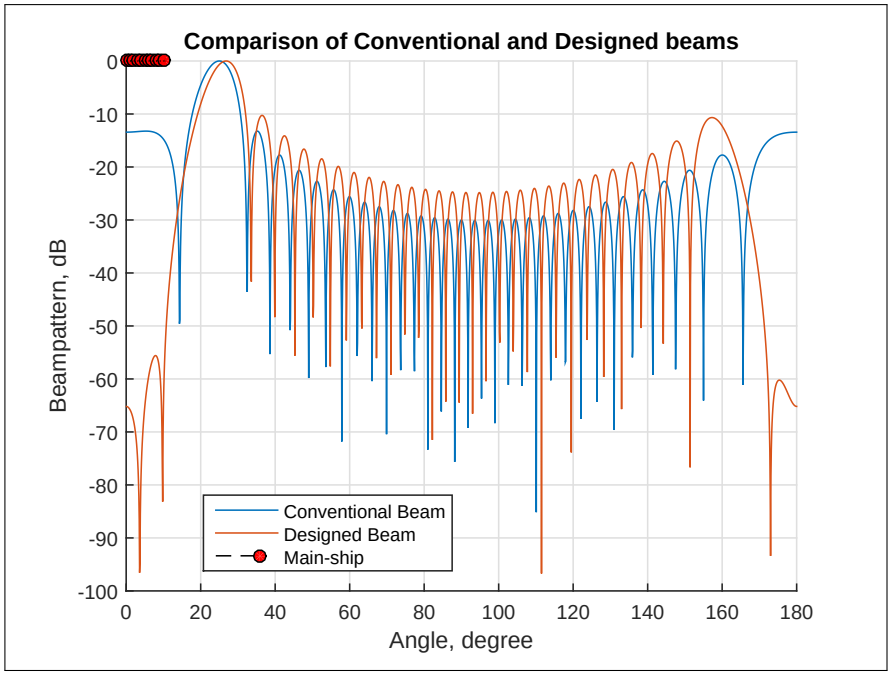

Figure 2.3: Comparison of designed and conventional beampatterns for SOI: 25°

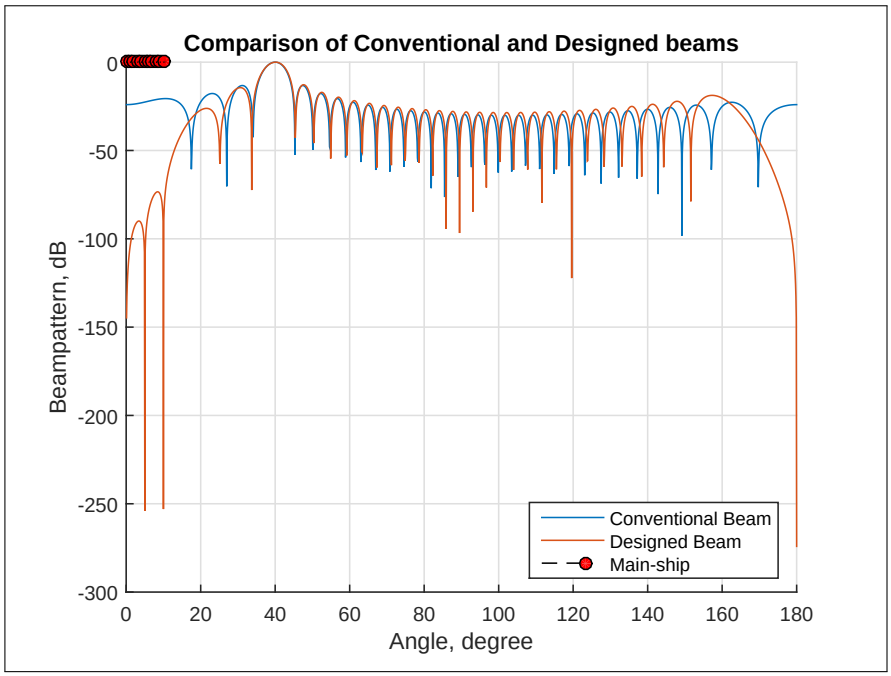

Figure 2.4: Comparison of designed and conventional beampatterns for SOI: 40°

CHAPTER 3

RESULTS

In this chapter, a comparison of the reduced dimension Worst-Case Performance Optimization with the conventional subspace and the designed subspace and the full dimensional adaptive and robust beamformer techniques (described in Chapter 2) is given. In the first section, simulation results are examined. Next, a performance comparison of these methods is made by using the field data of a towed array. Implementations of these methods and simulations are performed in MATLAB.

3.1 Simulation Results

In this section, the simulation results are given. In simulations, a uniform linear array with 32 sensors is used. For all simulations, the parameters and assumptions used are as follows:

- Sensors are omnidirectional.
- Sensors are spaced half of a wavelength apart.
- For all simulation results, 200 Monte Carlo runs are used.
- In order to emulate main-ship noise, 5 interfering sources are used with the direction of arrival angles and Interference to Noise Ratios (INR) given in Table 3.1.
- An interfering source with the direction of arrival 30° and INR = 30 dB is

used.

Table 3.1: Interfering sources to define main-ship noise

Angle, degree	2	4	6	8	10
INR, dB	30	25	20	18	14

- For all sources, far-field assumption (plane wavefronts) is used.
- For dimension reduction, 2 beams with 1 degree intervals are used for each side of the main beam (e.g. the conventional subspace in Figure 3.1).

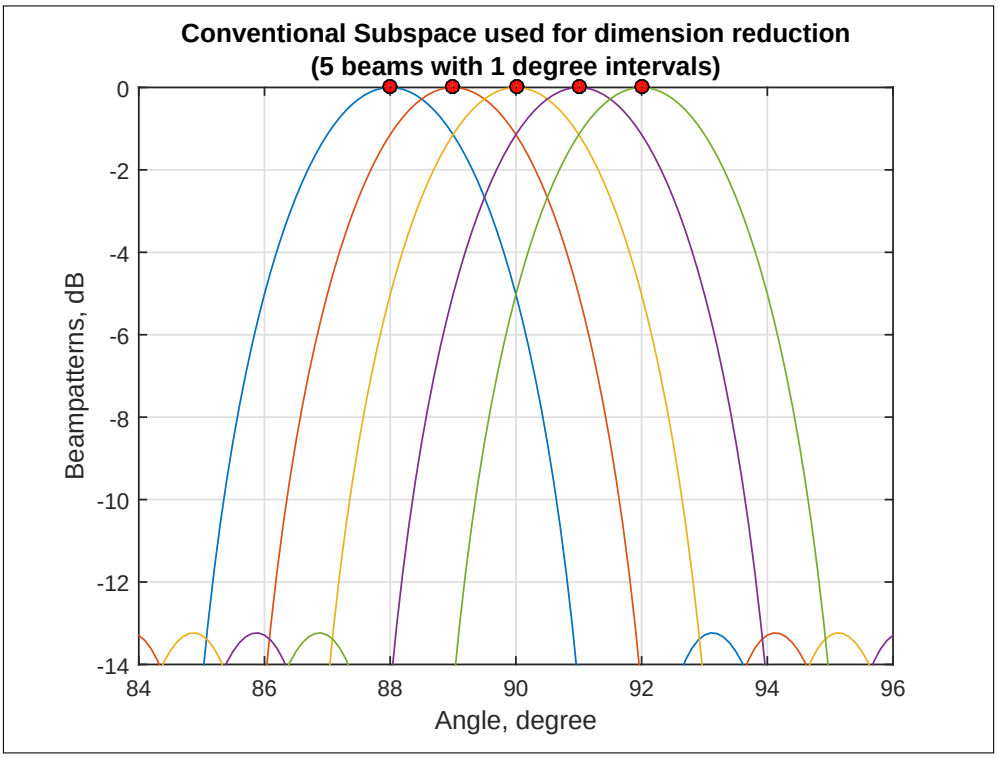

Figure 3.1: Conventional subspace used for dimension reduction, SOI: 90°, 5 beams with 1° intervals

In the next sections, the SMI beamformer, the full dimension WCO beamformer, the reduced dimension Worst-Case Performance Optimization Beamformer with the conventional subspace and the designed subspace are compared for different cases. First, the performance of each method under ideal case is examined. Then, signal look direction mismatch and sensor placement error are examined.

Lastly, performance of each method under coherent and incoherent local scattering of the signal is investigated.

3.1.1 Case 1: No Mismatch

In this case, the assumed and actual steering vectors are exactly the same and the sample covariance matrix is estimated using training snapshots $N = 64$. In order to determine the user parameter ε for the robust beamformer techniques, SINR values versus angle and epsilon are obtained. Figure 3.2, 3.3, and 3.4 display how the performance of each method is related to the user parameter ε. These figures are generated by shifting direction of arrival of SOI and by calculating SINR for each angle and epsilon, SNR= -10 dB for all cases. Using these figures, the proper epsilon values (red lines in figures) are selected to be used in all simulations.

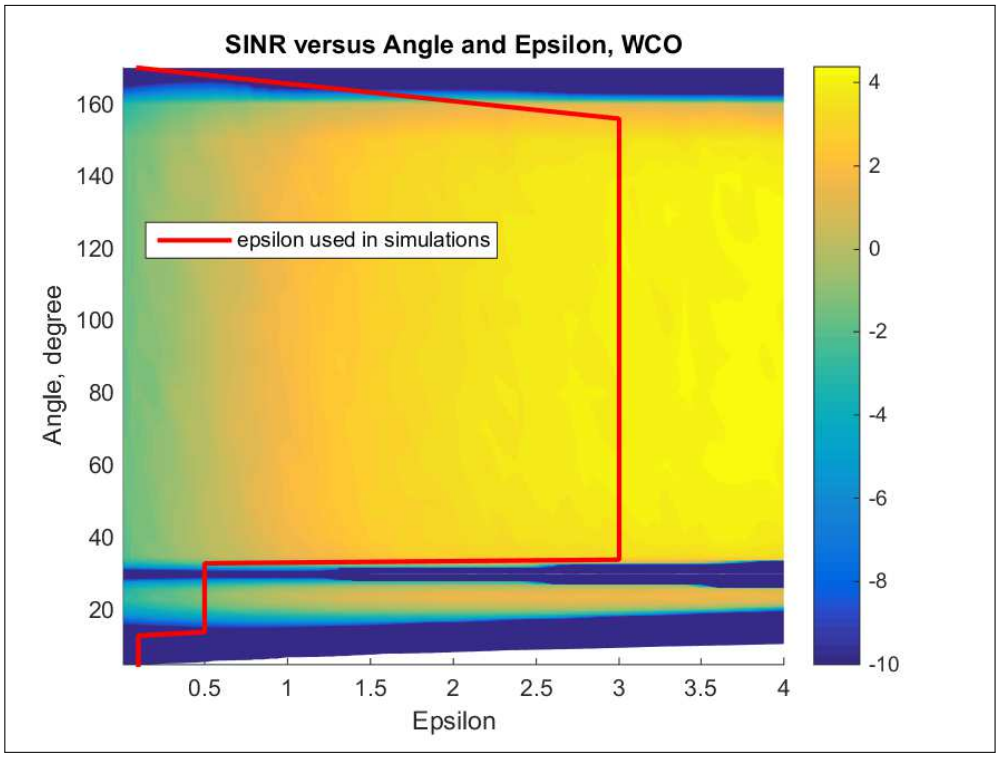

Figure 3.2: Output SINR versus epsilon and angle, Interferences: Main ship and 30° - Worst Case Optimization

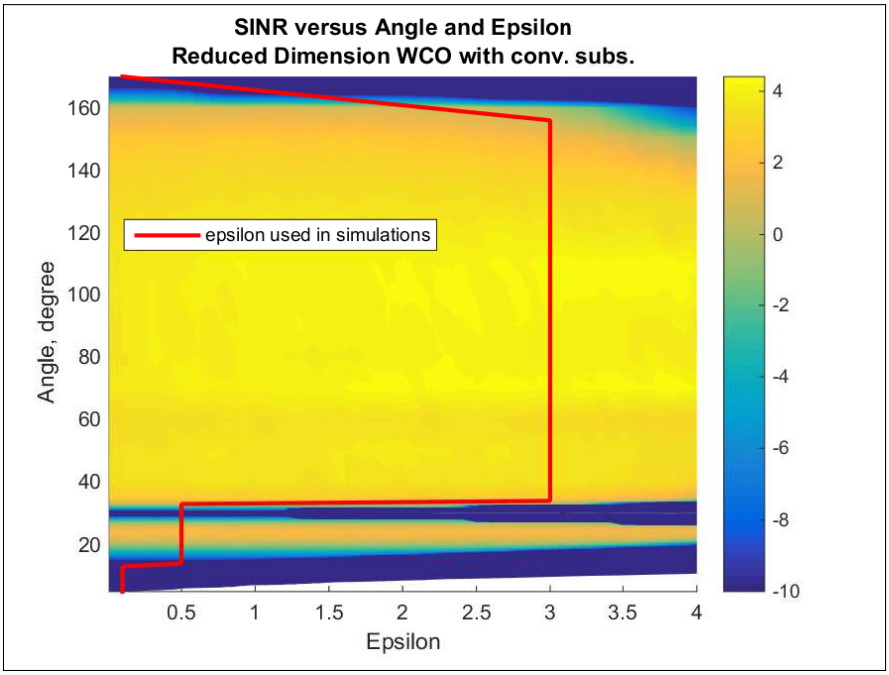

Figure 3.3: Output SINR versus epsilon and angle, Interferences: Main ship and 30° - Reduced Dimension Worst Case Optimization with conventional subspace

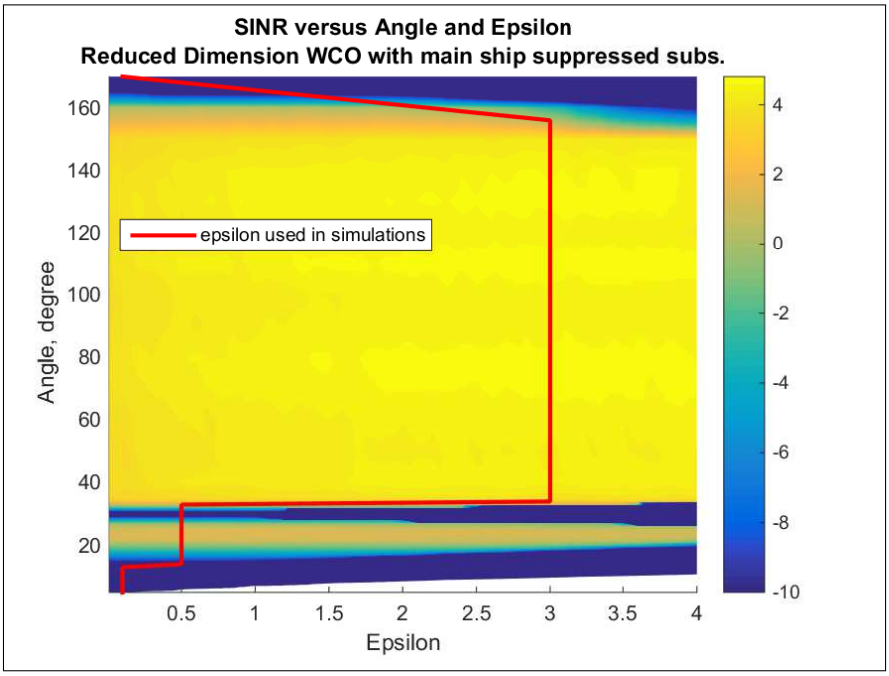

Figure 3.4: Output SINR versus epsilon and angle, Interferences: Main ship and 30° - Reduced Dimension Worst Case Optimization with main-ship suppressed subspace

Figure 3.5 shows the performance of each method with increasing number of snapshots for SOI that is impinging on the array at 90° and SNR = −10 dB. Robust methods perform well even with small number of snapshots compared to SMI. Moreover, the reduced dimension Worst Case Optimization Beamformer with main-ship suppressed subspace (nulled) performs better than other robust methods even with much smaller number of snapshots.

For all simulation results, the optimal beamformer output value and the performance bounds of the reduced dimension methods with both the conventional and the designed subspace are calculated by using the theoretical covariance matrix of interference plus noise.

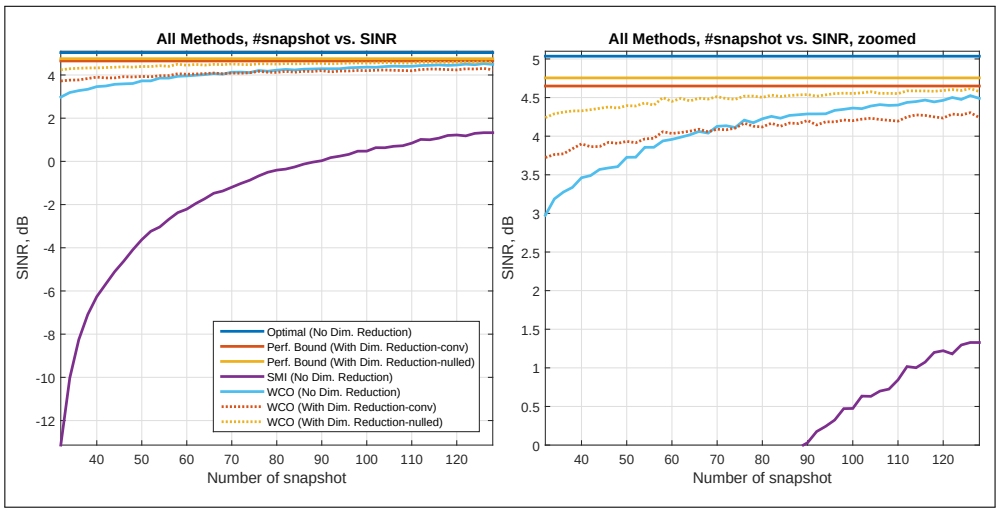

Figure 3.5: Output SINR versus number of snapshots, SOI: 90°, Interferences: Main ship and 30°

Beampatterns of each method for the ideal case (no mismatch) are given in Figure 3.6. As can be seen in the figure, the directions from where main-ship noise is impinging on the array are suppressed in the reduced dimension WCO that use the designed subspace for dimension reduction. Figure 3.7 displays output SINR with increasing SNR. Moreover, Figure 3.8 indicates the performance of methods in terms of bearings versus SINR for SNR = −10 dB and $N = 64$. As can be seen from Figure 3.6, 3.7, and 3.8 all robust methods perform much better than the Sample Matrix Inversion beamformer for small number of training snapshots. The reduced dimension WCO beamformer with main ship noise

suppressed subspace performs even better than the full dimension Worst Case Optimization beamformer.

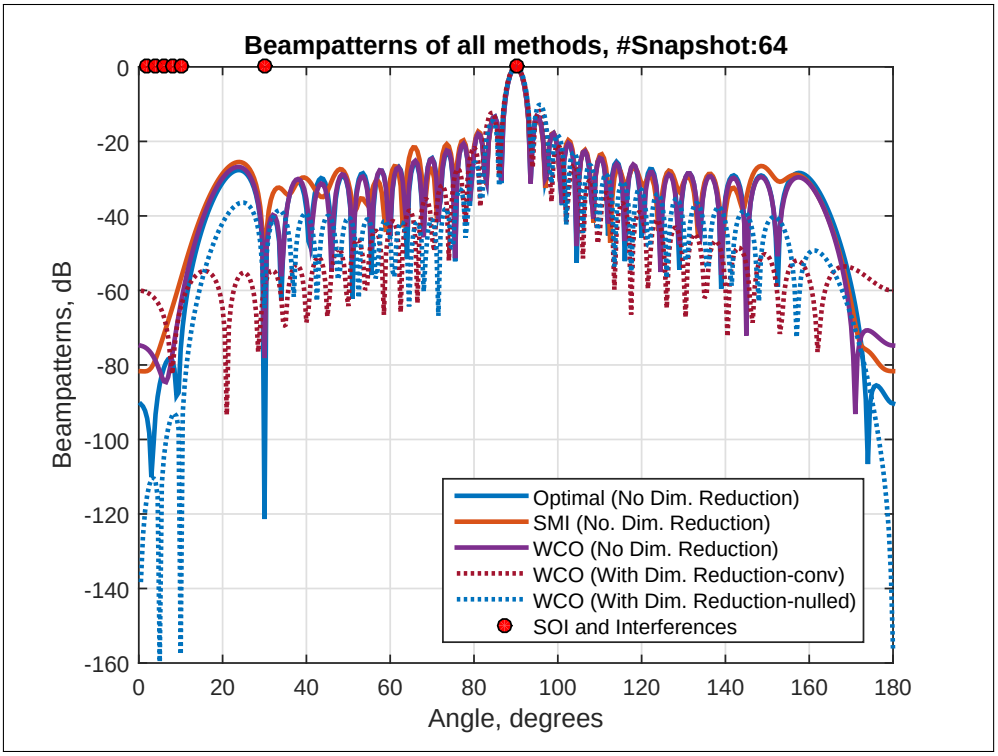

Figure 3.6: Beampatterns, $N = 64$, SOI: 90°, Interferences: Main ship and 30°

Note that in Figure 3.8, the performance bound of the reduced dimension method with the conventional subspace fluctuates near the interfering source at 30° and the performance bound of the reduced dimension WCO beamformer with main ship noise suppressed subspace has smaller oscillations. This is because of the fact that the reduced dimension WCO with the conventional subspace has less degrees of freedom. When the number of beams used in conventional subspace for dimension reduction is increased, as can be seen in Figure 3.9 the fluctuations decrease since degrees of freedom of this method are increased.

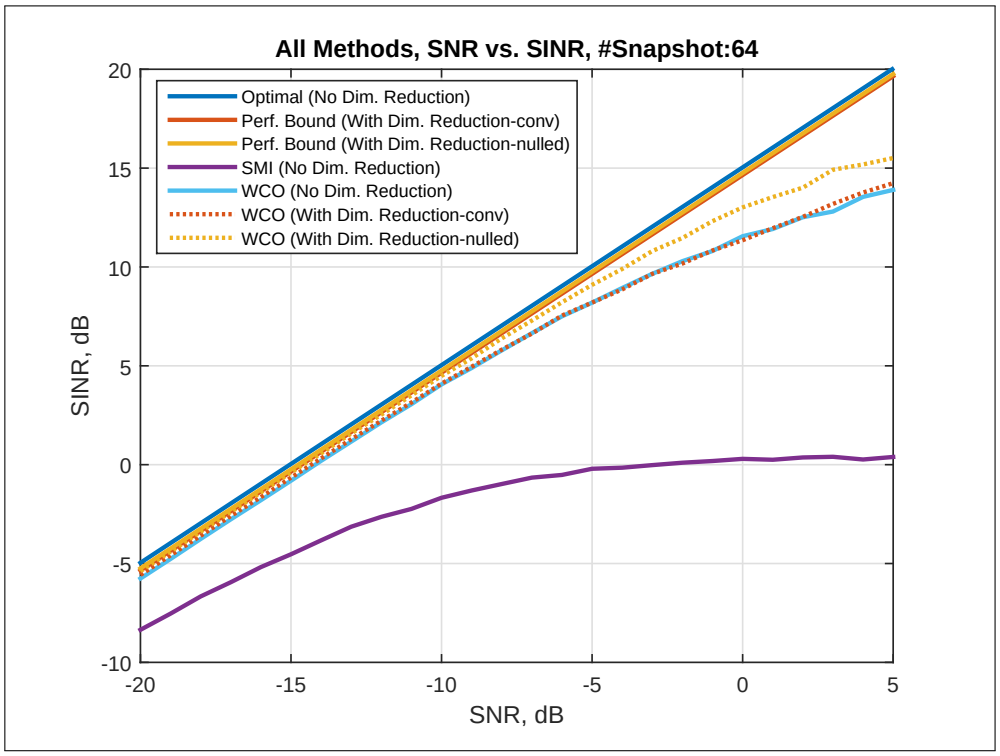

Figure 3.7: Output SINR versus SNR, SOI: 90°, Interferences: Main ship and 30°

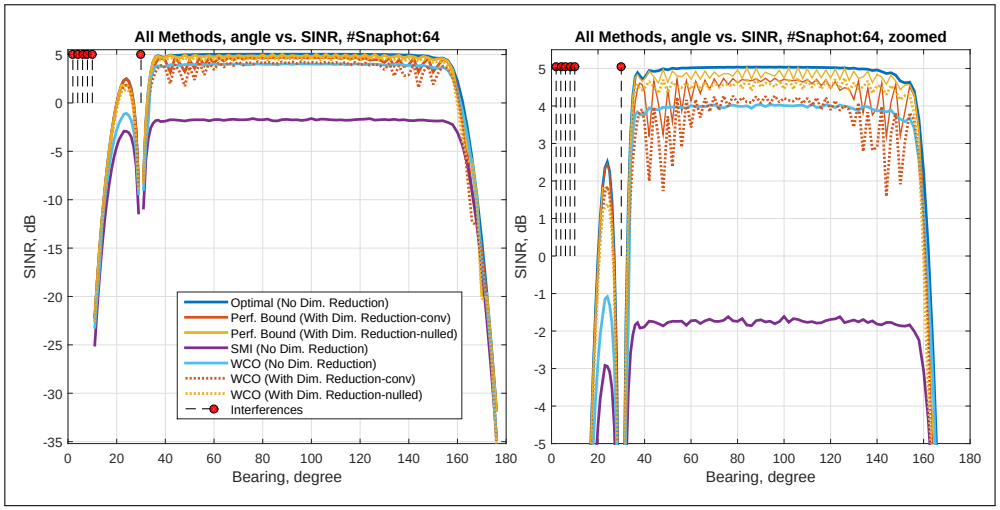

Figure 3.8: Output SINR for each bearing, Interferences: Main ship and 30°

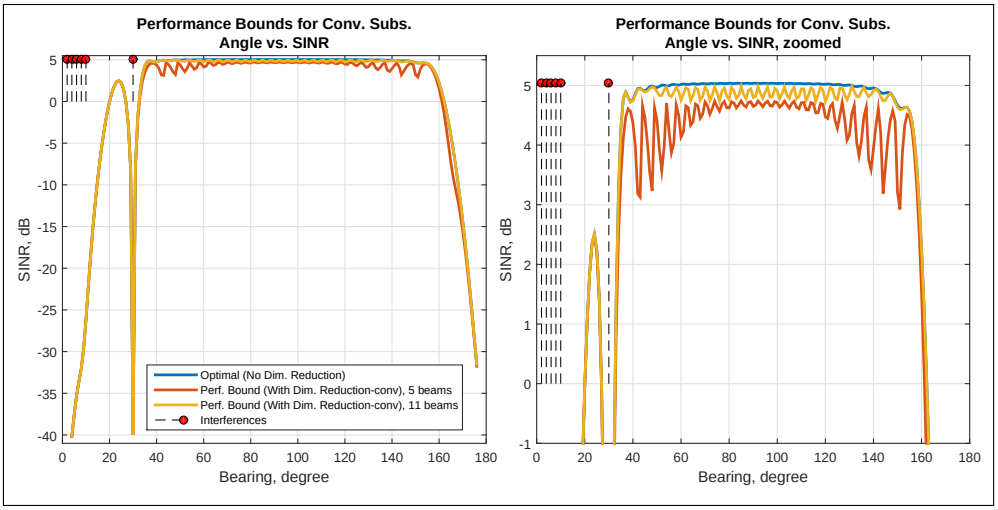

Figure 3.9: Comparison of performance bounds for the conventional subspace with 5 beams and 11 beams, Interferences: Main ship and 30°

3.1.2 Case 2: Array Look Direction Mismatch

As the second case, the look direction mismatch is considered. In this case, the SOI is impinging on the array from the DOA ϕ and the assumed steering vector is formed by using the DOA as $\phi + 1°$. This corresponds to a 1° look direction mismatch.

Figure 3.10 elaborates the performance of beamforming techniques with increasing number of training snapshots for the fixed SNR $= -10$ dB. It can be observed that the Sample Inversion Matrix beamformer tries to suppress the SOI as an interference instead of maintaining distortionless response. The robust methods have performance degradations but perform well compared to SMI especially the reduced dimension WCO beamformers.

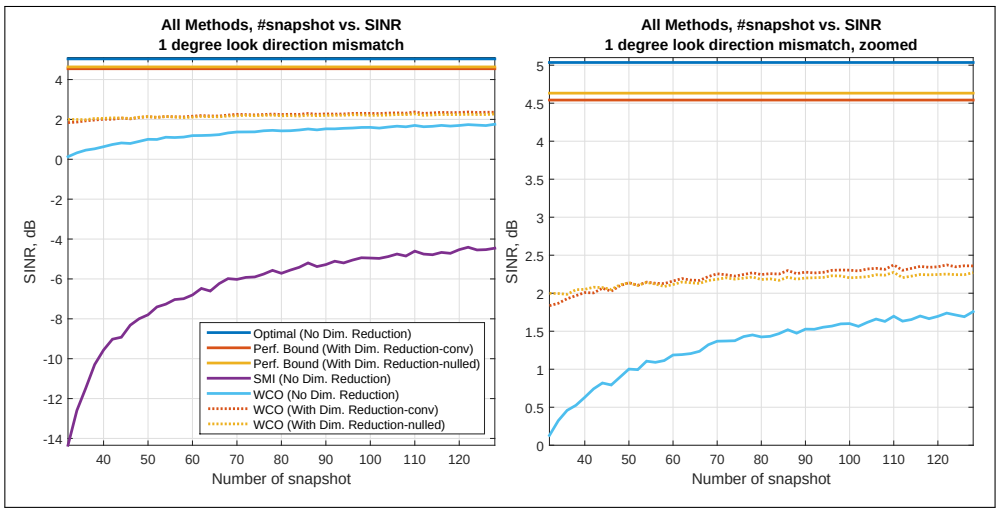

Figure 3.10: Output SINR versus number of snapshot, 1° look direction mismatch, SOI: 90°, Interferences: Main ship and 30°

Beampatterns of each method for 1° look direction mismatch case and the number of training snapshots $N = 64$ are given in Figure 3.11. It can also be seen from the beampatterns that the SMI beamformer tends to interpret the SOI as an interference. Moreover, the performance of these algorithms versus the SNR for this case is shown in Figure 3.12. At high SNR values, the performance of the SMI beamformer is worse than it is at low SNR values since the training snapshots are now contaminated by the SOI. Although robust methods also

have small performance degradation at high SNR values, their performances are much higher than the SMI beamformer.

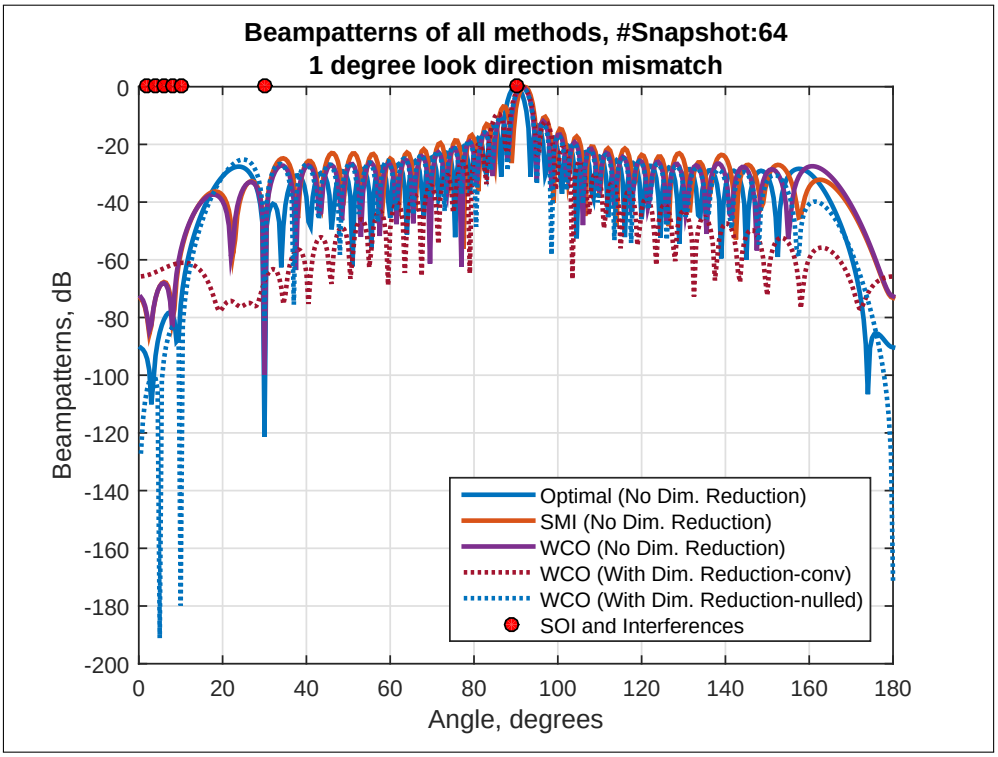

Figure 3.11: Beampatterns, 1° look direction mismatch, SOI: 90°, Interferences: Main ship and 30°

Figure 3.13 indicates the performance of methods in terms of bearings versus SINR for SNR $= -10$ dB and $N = 64$. The reduced dimension WCO with the subspace that main ship noise suppressed has best performance for each bearing under the small number of training snapshots and 1° look direction mismatch.

The performance results in this section are generated by using the user parameter ϵ which is determined in no mismatch case. For the number of training snapshots $N = 64$ and 1° look direction mismatch, the epsilon analysis for the reduced dimension WCO with the subspace that main ship noise suppressed is recalculated and the ϵ values for each bearing is updated (red line in Figure 3.14).

In Figure 3.15, the performance of the reduced dimension WCO with the subspace that main ship noise suppressed in terms of bearings versus SINR for the

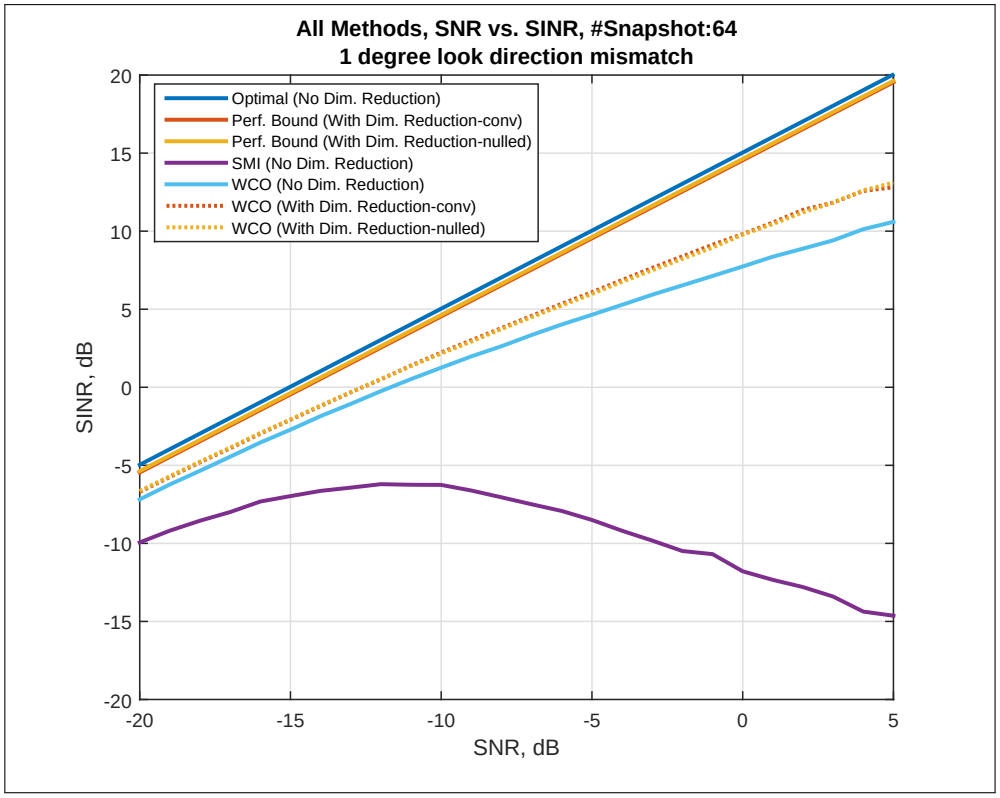

Figure 3.12: Output SINR versus SNR, 1° look direction mismatch, SOI: 90°, Interferences: Main ship and 30°

epsilon set determined in no mismatch case and in this case is given in Figure 3.15. By using the updated epsilon values, the SINR at the output of this beamformer is increased.

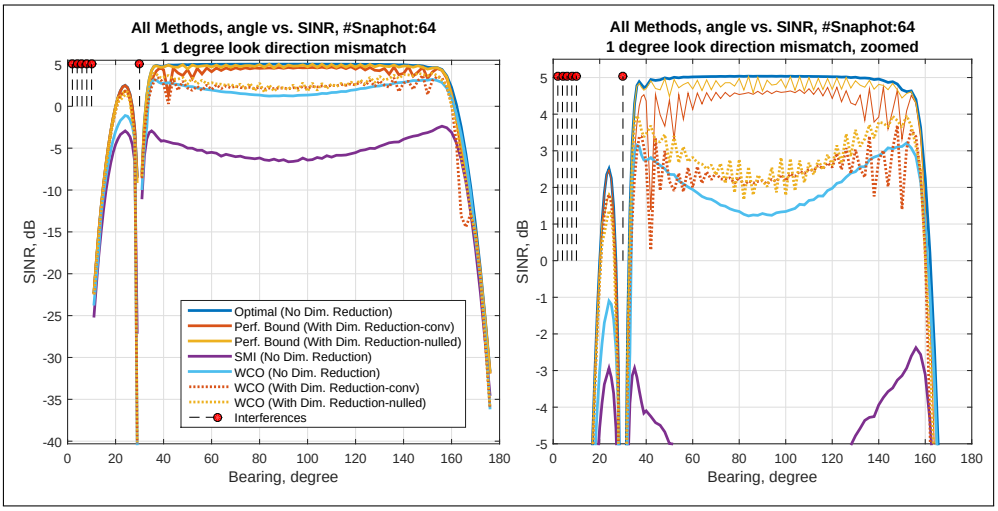

Figure 3.13: Output SINR for each bearing, 1° look direction mismatch, Interferences: Main ship and 30°

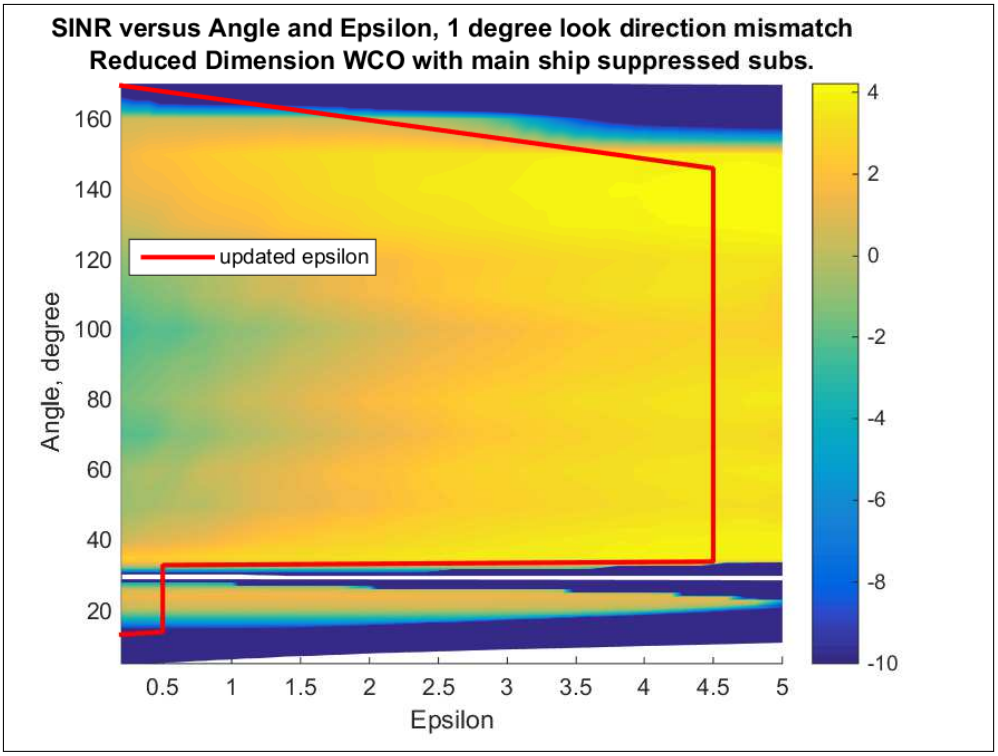

Figure 3.14: Output SINR versus epsilon and angle, 1° look direction mismatch, Interferences: Main ship and 30°, - Reduced Dimension Worst Case Optimization with main-ship suppressed subspace

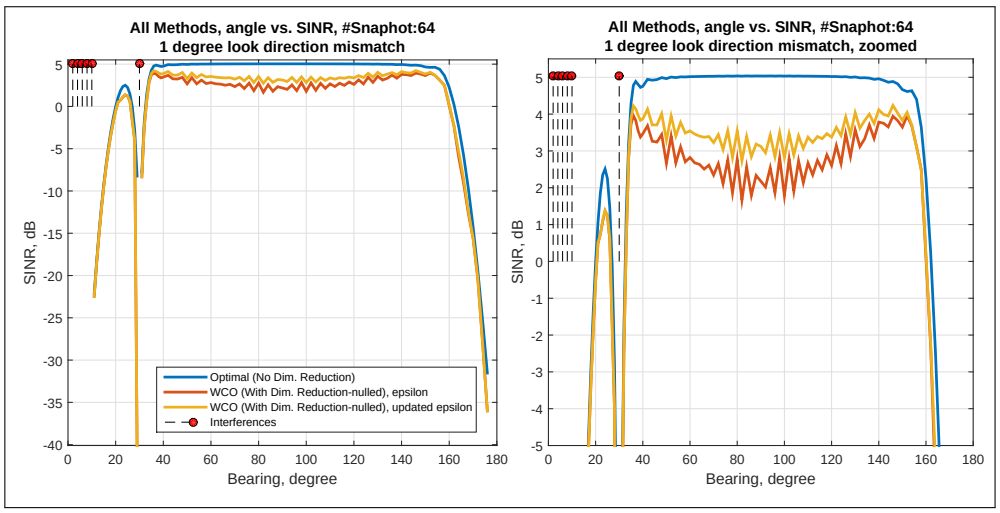

Figure 3.15: Output SINR versus angle for updated epsilon values, 1° look direction mismatch, Interferences: Main ship and 30°, - Reduced Dimension Worst Case Optimization with main-ship suppressed subspace

3.1.3 Case 3: Sensor Placement Error

Sensor placement error is considered as the next case. In this case, the assumed steering vector is formed by using the designed sensor positions; but the true steering vector is different from the assumed steering vector. Uniformly drawn sensor placement error from the interval [-0.01λ, 0.01λ] is added to the designed sensor positions when the array output is generated in simulations. Note that the sensor placement error is changed in each Monte Carlo run.

The performance of the beamforming techniques with increasing the number of training snapshots for the fixed SNR $= -10$ dB is shown in Figure 3.16. In this case, the performance of the reduced dimension methods is worse than the full dimension WCO beamformer since the design of the subspaces used to reduce dimension also comprises the sensor placement error. However, they still have much higher performance compared to the SMI beamformer especially for small number of training snaphots.

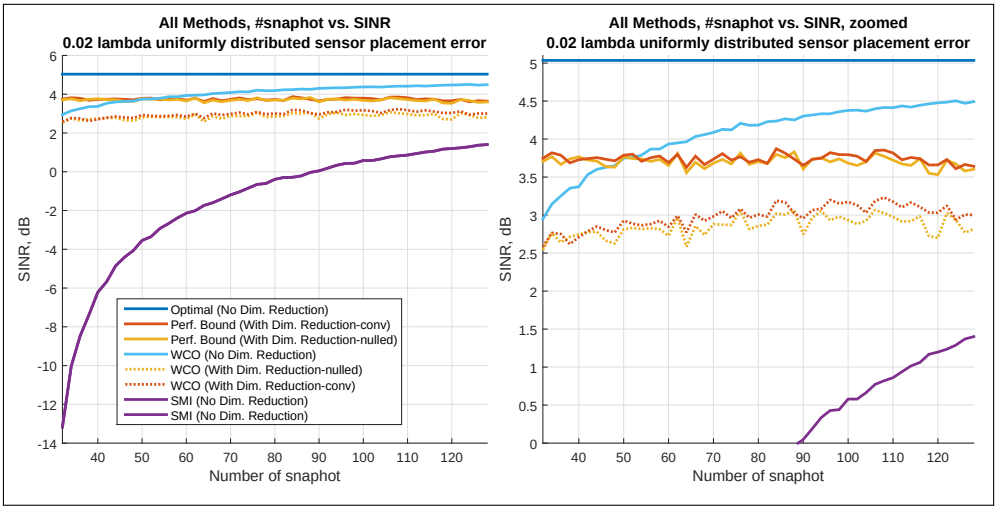

Figure 3.16: Output SINR versus number of snapshot, [-0.01λ 0.01λ] uniformly distributed sensor placement error, SOI: 90°, Interferences: Main ship and 30°

Beampatterns of methods and the performance of these algorithms versus the SNR for uniformly drawn sensor placement error from the interval ([-0.01λ, 0.01λ]) and the number of training snapshots $N = 64$ are given in Figure 3.17 and 3.18, respectively. With increasing SNR, the performance difference between

the reduced dimension WCO beamformers and full dimension WCO beamformer decreases. At high SNR values, the reduced dimension methods perform as good as the full dimension WCO beamformer.

Lastly, the performance of methods in terms of bearing versus SINR for SNR $= -10$ dB and $N = 64$ is displayed in Figure 3.19. Although reduced dimension methods have performance degradations compared to the full dimension WCO beamformer at angle interval [30° 160°], they are better than the full dimension WCO and much better than the SMI beamformer at angle interval [20° 30°] between the interferences.

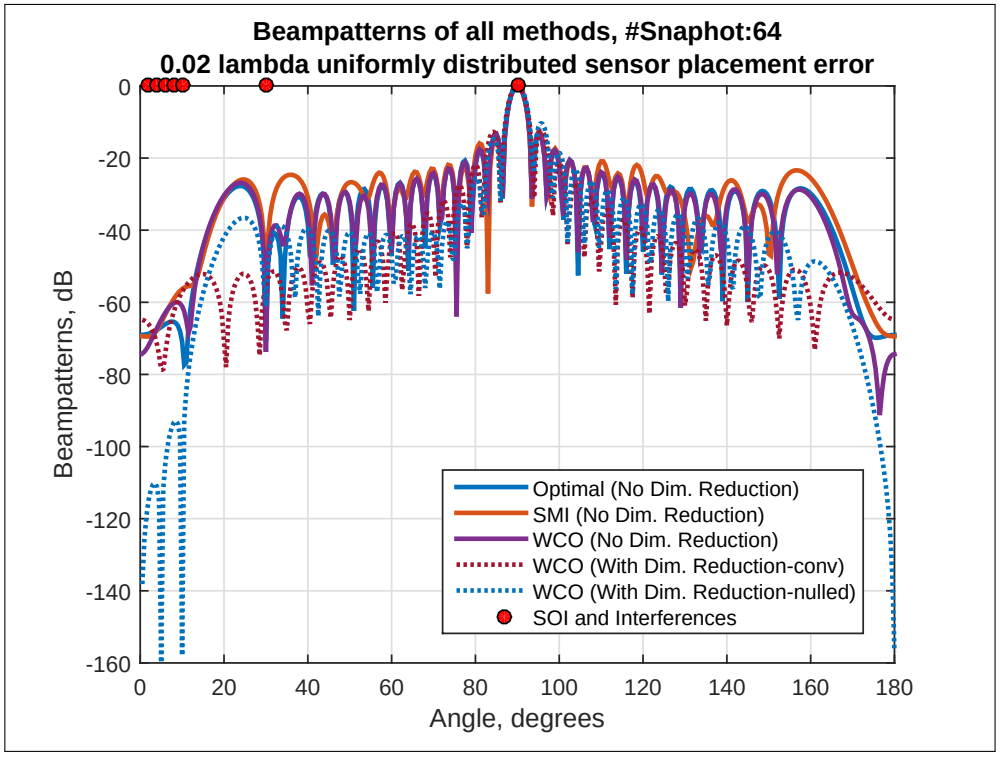

Figure 3.17: Beampatterns, [-0.01λ 0.01λ] uniformly distributed sensor placement error, SOI: 90°, Interferences: Main ship and 30°

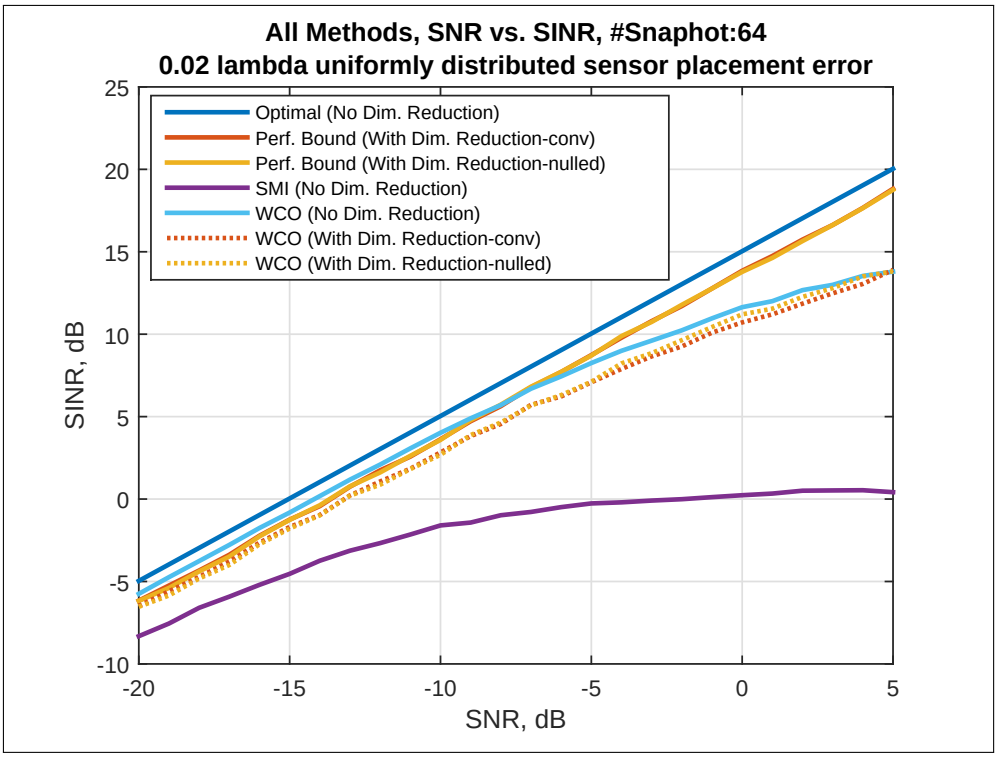

Figure 3.18: Output SINR versus SNR, [-0.01λ 0.01λ] uniformly distributed sensor placement error, SOI: 90°, Interferences: Main ship and 30°

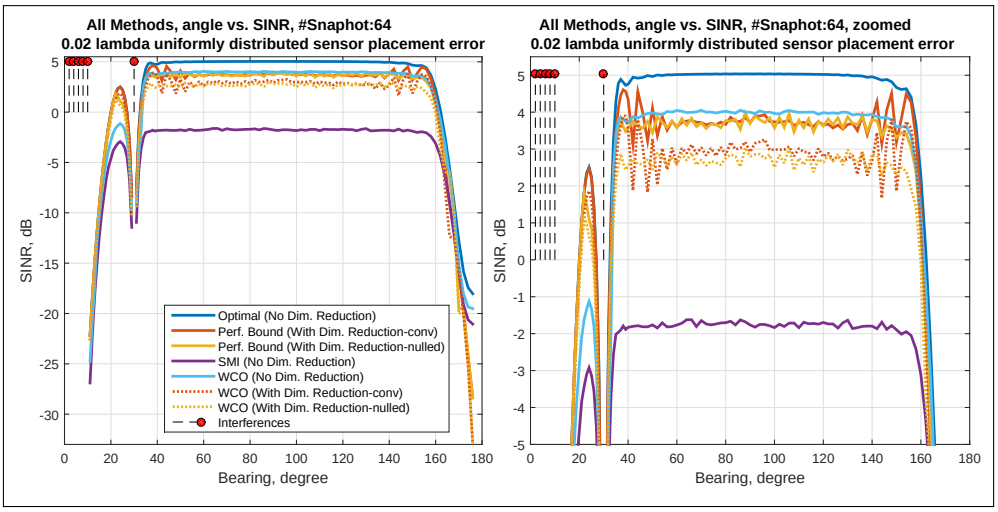

Figure 3.19: Output SINR for each bearing, [-0.01λ 0.01λ] uniformly distributed sensor placement error, Interferences: Main ship and 30°

3.1.4 Case 4: Coherent Local Scattering

In this case, the spatial signature of the SOI is distorted by local scattering effects that are defined as plane waves impinging on array from the 3 different paths. That is, the actual spatial signature is coming to the array by four signal paths given by

$$\tilde{\mathbf{a}}(\phi_0) = \mathbf{a}(\phi_0) + \sum_{i=1}^{3} e^{j\psi_i}\mathbf{a}(\phi_i) \tag{3.1}$$

where $\mathbf{a}(\phi_0)$ is the assumed steering vector corresponding to direct path and $\mathbf{a}(\phi_i)$ $(i = 1, 2, 3)$ are steering vectors corresponding to the coherently scattered paths. Angles ϕ_i of the coherently scattered paths are independently drawn from a uniform random distribution with mean= ϕ_0 and standard deviation= 1° and phases ψ_i are also independently and uniformly drawn from the interval $[0\ 2\pi]$ in each Monte Carlo run. That is, angles and phases of the scatters remained frozen from snapshot to snapshot and are changed from run to run. Note that all signal paths are used to calculate the SNR in this case when the array output is generated in simulations.

The performance of the methods with increasing number of training snapshots for the fixed SNR $= -10$ dB is given in Figure 3.20. In Figure 3.21, the beampatterns of methods are displayed for fixed the number of training snapshots $N = 64$ and SNR $= -10$ dB. Additionally, the performance of these methods versus SNR for the training snapshots $N = 64$ is compared in Figure 3.22. As a last result for this case, the performance of methods in terms of bearings versus SINR for SNR $= -10$ dB and $N = 64$ is given in Figure 3.23. As can be seen from the results given for this case, the reduced dimension WCO beamformer with the designed subspace has the best performance among all the other methods tested.

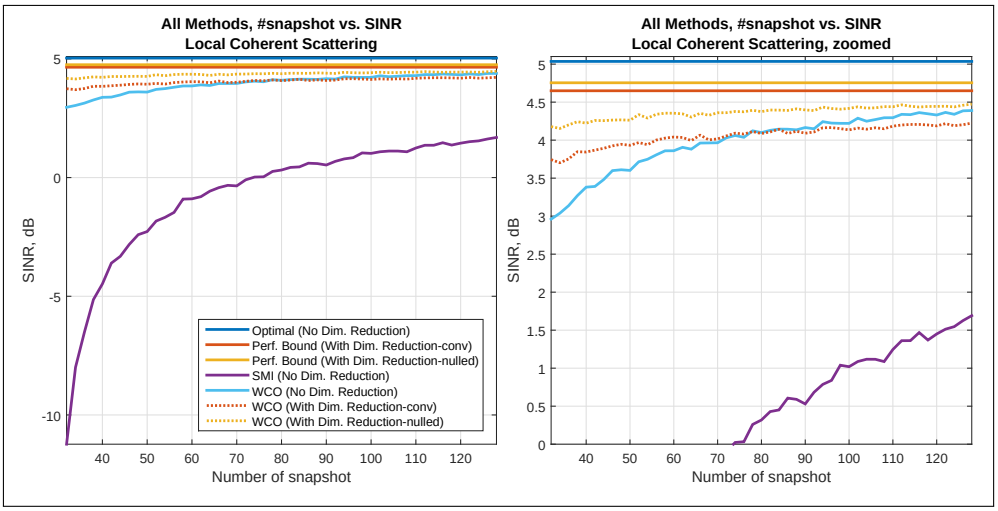

Figure 3.20: Output SINR versus number of snapshot, Local Coherent Scattering, SOI: 90°, Interferences: Main ship and 30°

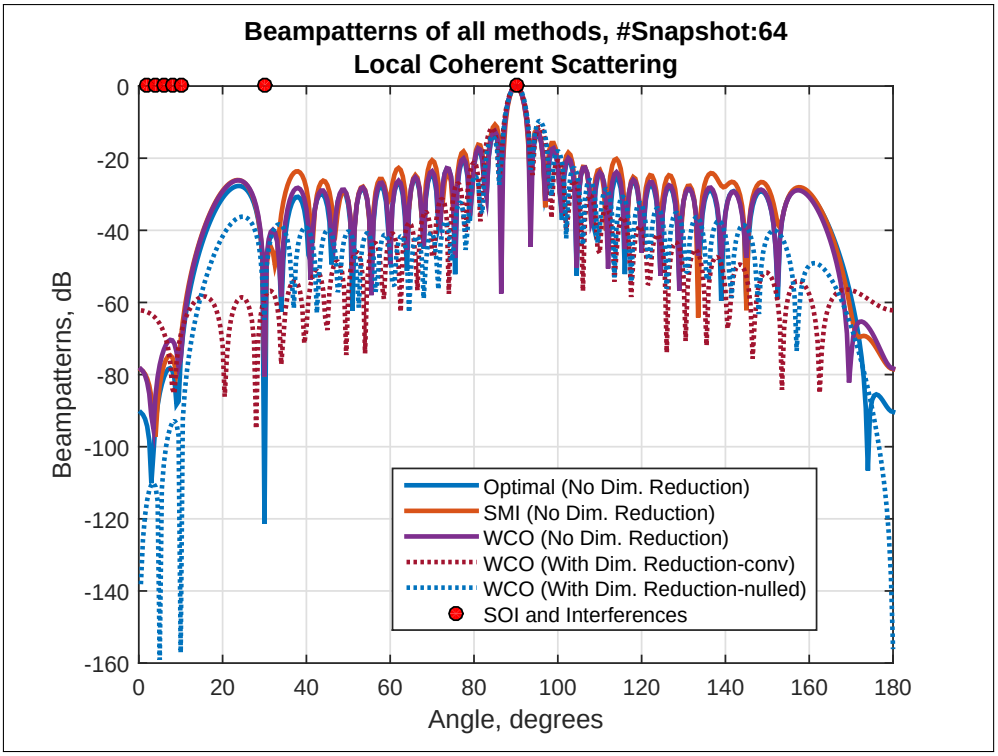

Figure 3.21: Beampatterns, Local Coherent Scattering, SOI: 90°, Interferences: Main ship and 30°

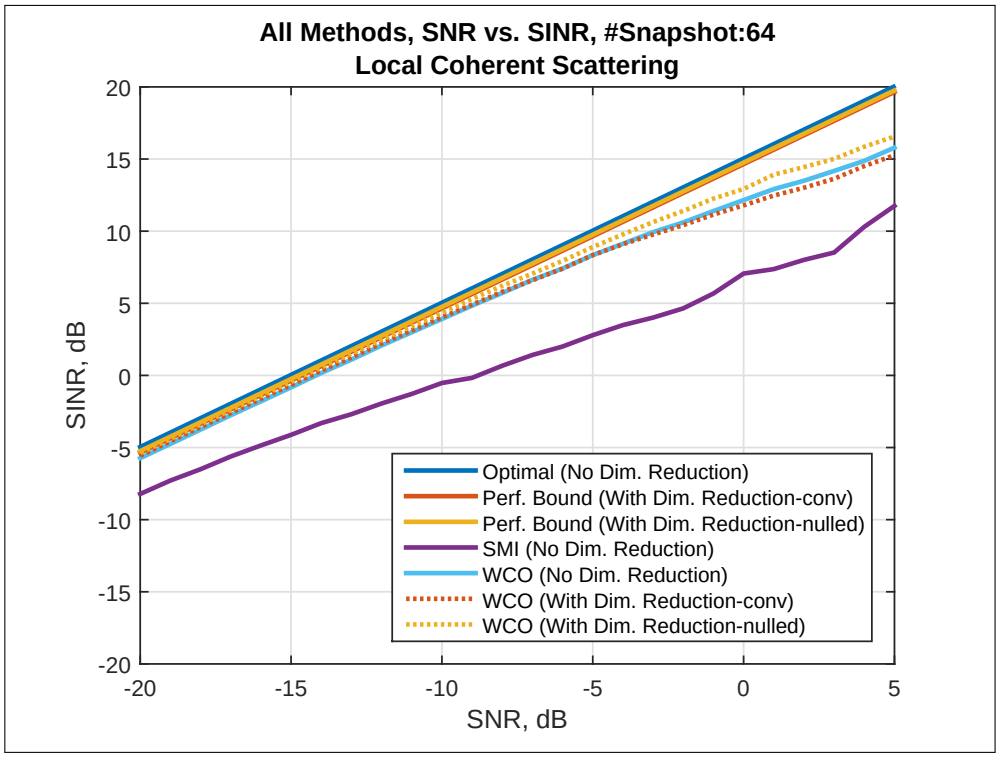

Figure 3.22: Output SINR versus SNR, Local Coherent Scattering, SOI: 90°, Interferences: Main ship and 30°

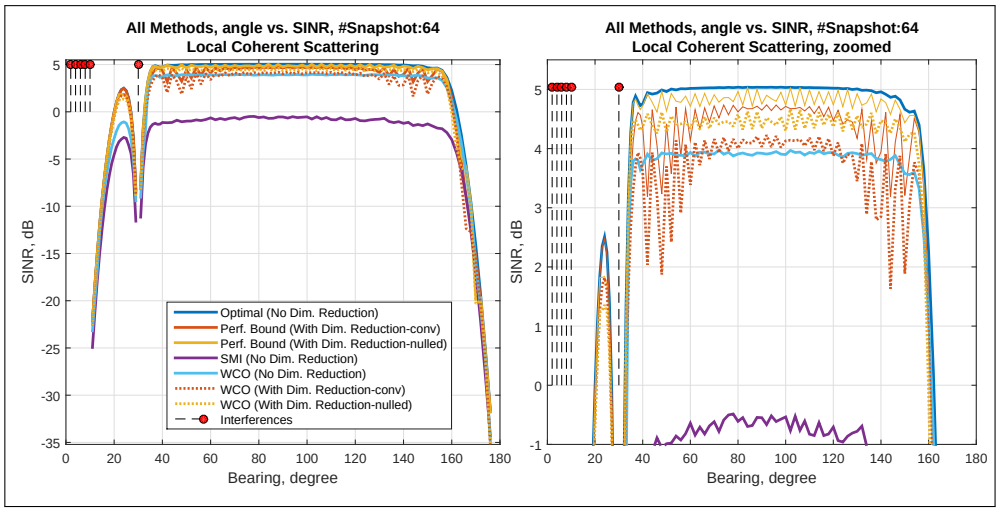

Figure 3.23: Output SINR for each bearing, Local Coherent Scattering, Interferences: Main ship and 30°

3.1.5 Case 5: Incoherent Local Scattering

As a final case, the case of incoherent local scattering is considered. In this case, the spatial signature of the SOI is time-varying and is modeled by

$$\tilde{s}(t) = s_0(t)\mathbf{a}(\phi_0) + \sum_{i=1}^{3} s_i(t)\mathbf{a}(\phi_i) \tag{3.2}$$

where the angles ϕ_i $(i = 1, 2, 3)$ are independently drawn from a uniform random distribution with mean= ϕ_0 and standard deviation= 1°, $s_i(t)$ are i.i.d. zero-mean complex Gaussian variables. In order to define incoherent local scatterers, ϕ_i is changed in each Monte Carlo and remained fixed from snapshot to snapshot while $s_i(t)$ is changed both from snapshot to snapshot and from run to run. As in the previous case, all signal paths are used to calculate the SNR as the array output is generated in simulations. Note that, according to the signal model (3.2), the covariance matrix of the SOI R_s is no longer a rank-one matrix.

As a first simulation result, similar to previous cases, the performance of methods versus the number of training snapshots for SNR $= -10$ dB is given in Figure 3.24. In Figure 3.25, beampatterns are shown for the training snapshots $N = 64$ and in Figure 3.26, the output SINR values of methods versus SNR is presented when $N = 64$. Moreover, the dependency of the output SINR values to the DOA of SOI for $N = 64$ and SNR $= -10$ dB is indicated in Figure 3.27. The given results show that the reduced dimension WCO with main ship noise suppressed subspace provide advantage against the incoherent local scatterers.

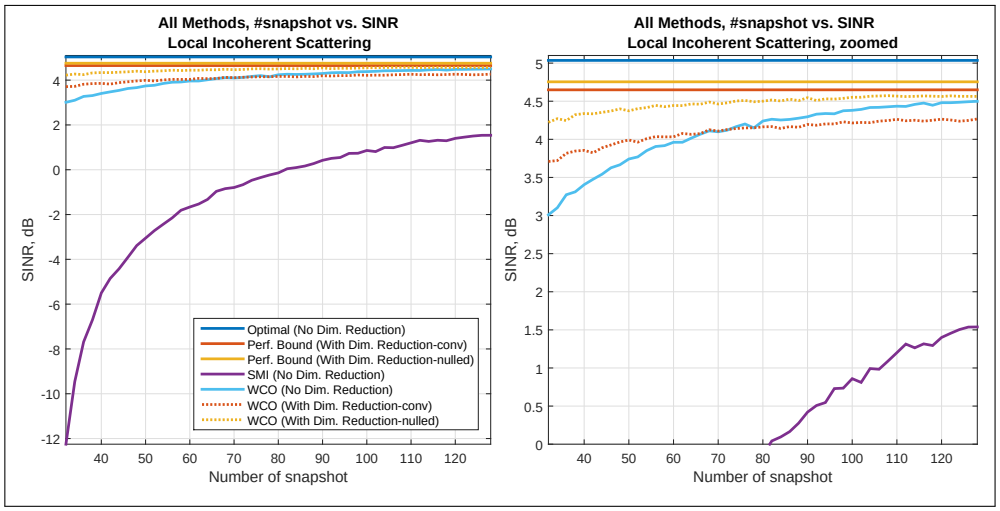

Figure 3.24: Output SINR versus number of snapshot, Local Incoherent Scattering, SOI: 90°, Interferences: Main ship and 30°

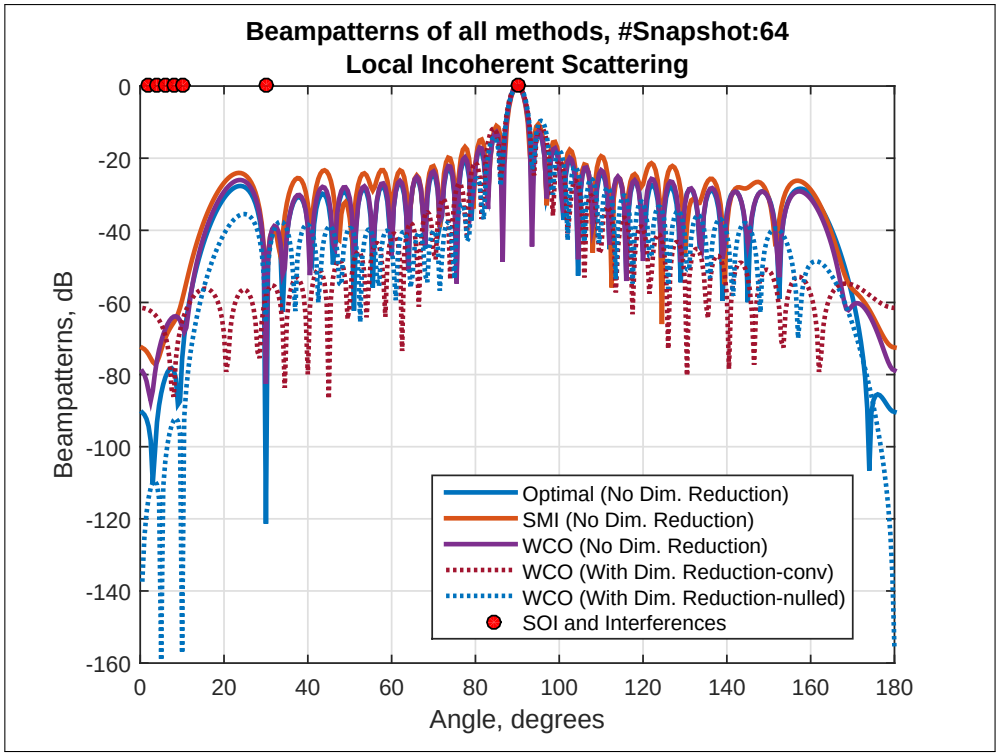

Figure 3.25: Beampatterns, Local Incoherent Scattering, SOI: 90°, Interferences: Main ship and 30°

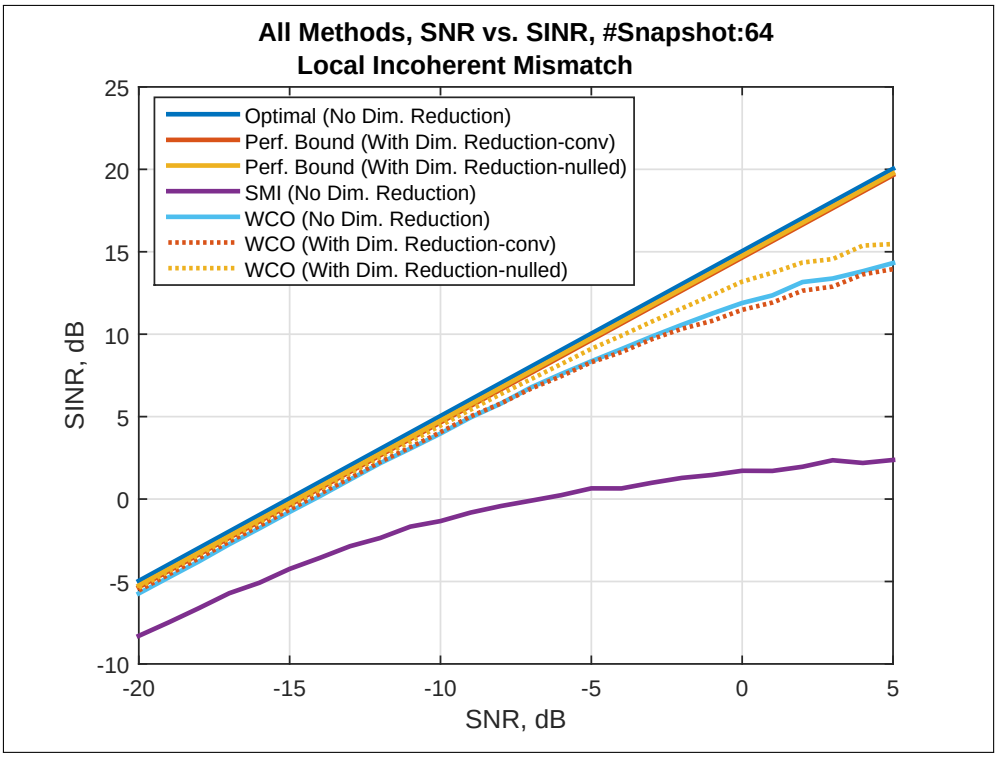

Figure 3.26: Output SINR versus SNR, Local Incoherent Scattering, SOI: 90°, Interferences: Main ship and 30°

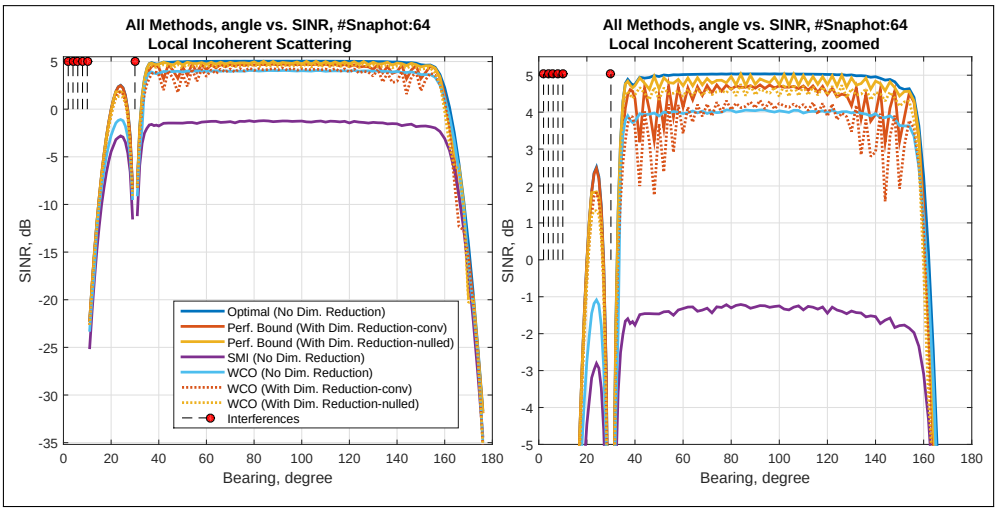

Figure 3.27: Output SINR for each bearing, Local Incoherent Scattering, Interferences: Main ship and 30°

3.2 Experimental Results

In this section, a performance comparison of each beamforming method is made using the passive sonar data collected with a large towed array during the sea trials of ASELSAN in the Marmara Sea.

To compute the beamformer outputs, 32 sensors spaced half wavelength apart of the towed array are used. The parameters of the towed array such as design frequency, total number of sensors, array length are proprietary. The sensor outputs were %50 overlapped and fast Fourier transformed (FFT). The lengths of the overlapping windows were selected to satisfy the bandwidth limit $B < \frac{1}{8T_{tr}}$ given in [2] where T_{tr} is the transit time across the towed array. Results are examined for a single frequency bin such that the center of the selected frequency bin corresponds to the design frequency of array. Moreover, the number of the frequency-domain training snapshots is equal to 63 and the snapshots are highly contaminated by the SOIs. The results are generated in only azimuth plane with angle separation 2.5°. That is, 72 beams are formed in the azimuthal plane.

While selecting the dataset, we pay attention the dataset to contain the weak sources in order to observe the performance of the methods at low SNR values and the strong sources to compare the interference rejection capability of methods. Moreover, it is remarked that the dataset has the source near the main ship noise and that provides to observe the performance of the designed subspace.

Bearing Time Records (BTRs) are given for the following methods

- Conventional Beamformer in Figure 3.28,
- SMI Beamformer in Figure 3.29,
- Worst-Case Performance Optimization Beamformer in Figure 3.30,
- Reduced Dimension Worst-Case Performance Optimization Beamformer with the conventional subspace in Figure 3.31,
- Reduced Dimension Worst-Case Performance Optimization Beamformer with the designed (nulled) subspace in Figure 3.32.

From the BTR figures, the following observations are made;

- It is clear that the Conventional Beamformer has the poorest performance. The weak sources at angles $60°, 100°, 110°, 125°$ in the first sample time cannot be observed in the BTR figure, as this beamformer does not have an adaptive interference rejection capability, high sidelobes of the strong sources like the main-ship noise between angles [160° 180°] mask these weak sources.

- The SMI Beamformer has better performance compared to the Conventional Beamformer. The weak sources now appear in the BTR figure owing to the improved interference rejection capability of this beamformer. However, the power of all the sources are weaker than the full dimension WCO beamformer. This is because of the fact that the SMI beamformer is not robust against the mismatches and other errors in real data. Also the performance degrades by the contaminated small number of training snapshots.

- The Worst-Case Performance Optimization Beamformer has the best performance among the full dimension methods tested since it is robust to mismatches, other modeling errors and even the small number of training snapshots. Only the source near to main-ship noise can barely be seen because of the strong source, main ship noise.

- Reduced Dimension Worst-Case Performance Optimization Beamformer with the conventional subspace has smaller performance degradation compared to the full dimension WCO beamformer but has better performance compared to the SMI beamformer. The output powers of sources are slightly decreased and the source near the main ship noise still cannot be observed clearly.

- Reduced Dimension Worst-Case Performance Optimization Beamformer with the designed (nulled) subspace performs as good as the full dimension WCO beamformer. Now, all sources, especially the source near the main ship noise, can be seen clearly. It can be seen that the use of the designed

subspace instead of the conventional subspace to reduce dimension has some advantages. These advantages are the stronger output power of sources and the more degrees of freedom. However, it is seen that the background noise in this reduced dimension method is slightly increased.

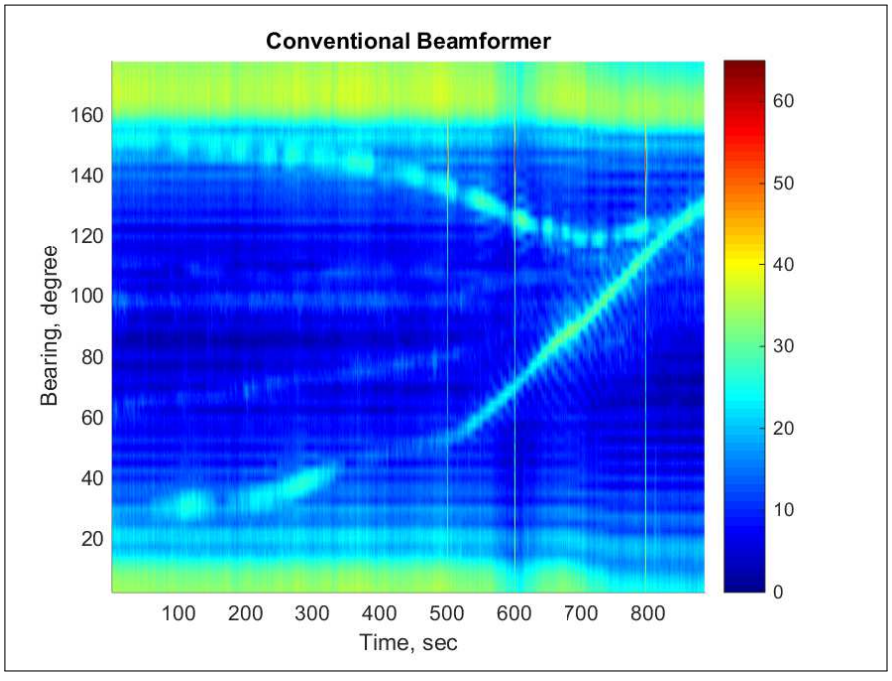

Figure 3.28: Bearing Time Record, Conventional Beamformer

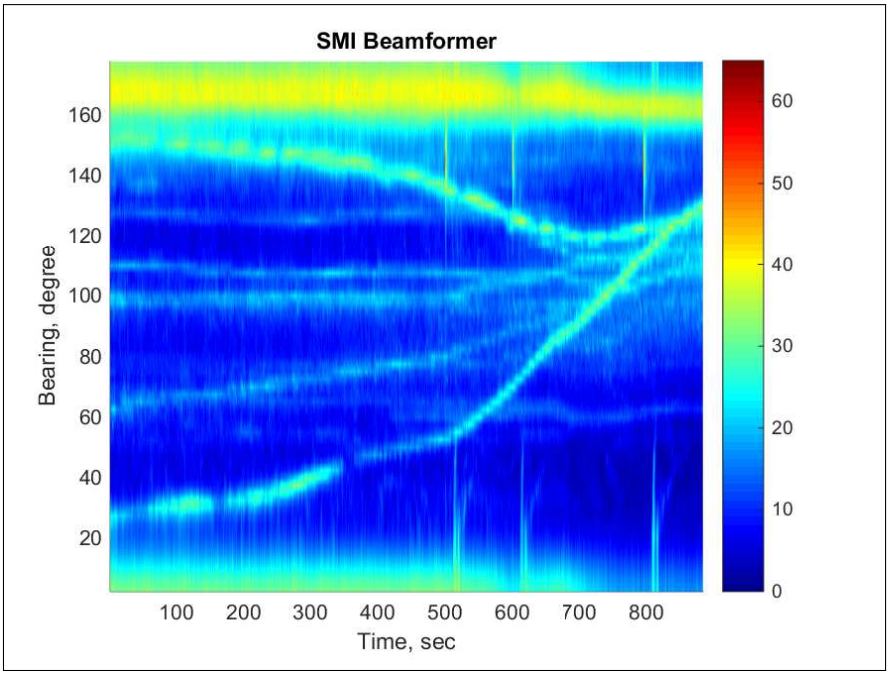

Figure 3.29: Bearing Time Record, SMI Beamformer

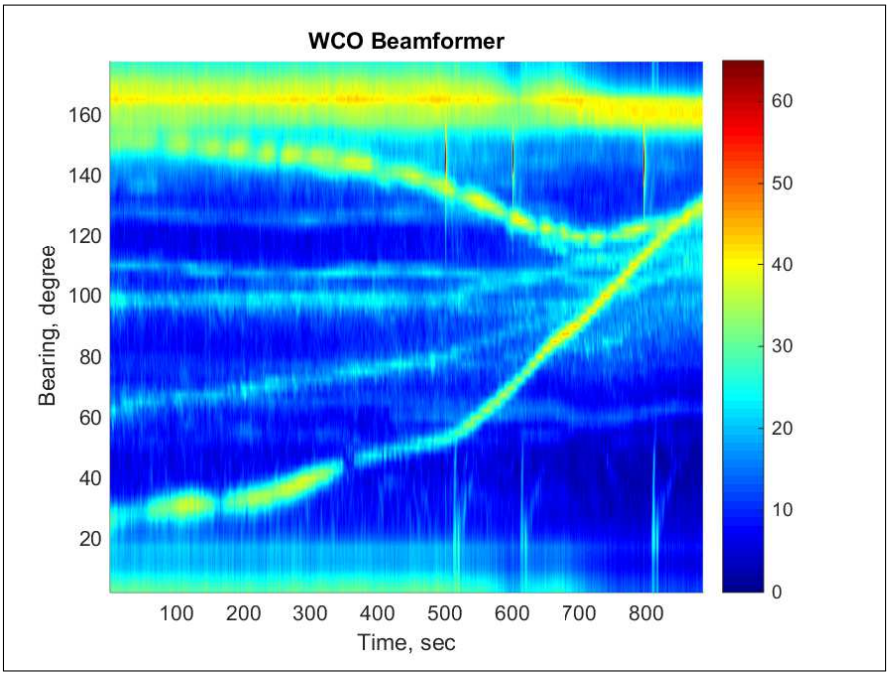

Figure 3.30: Bearing Time Record, WCO Beamformer

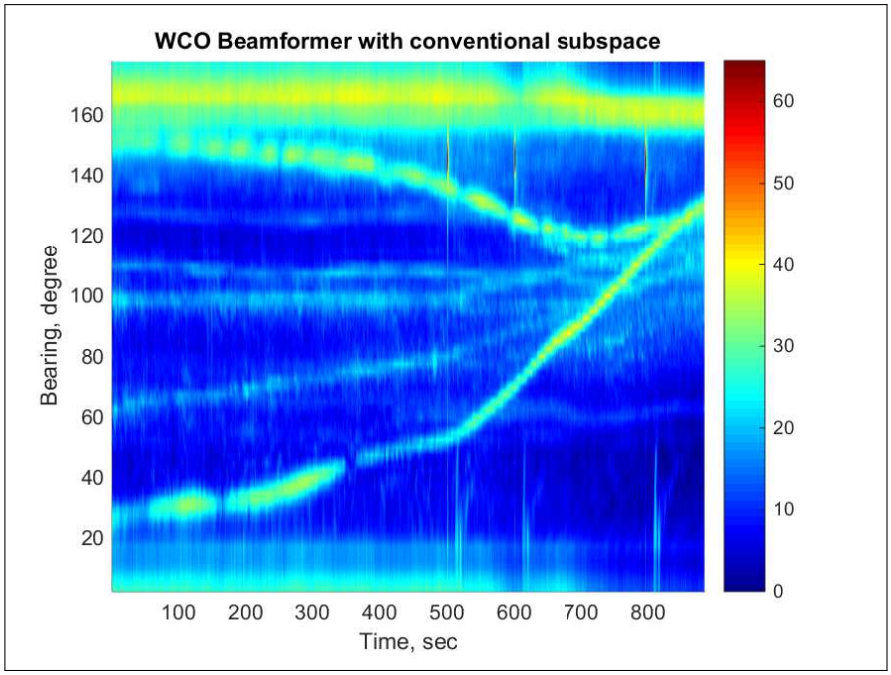

Figure 3.31: Bearing Time Record, Reduced Dimension WCO with the conventional subspace

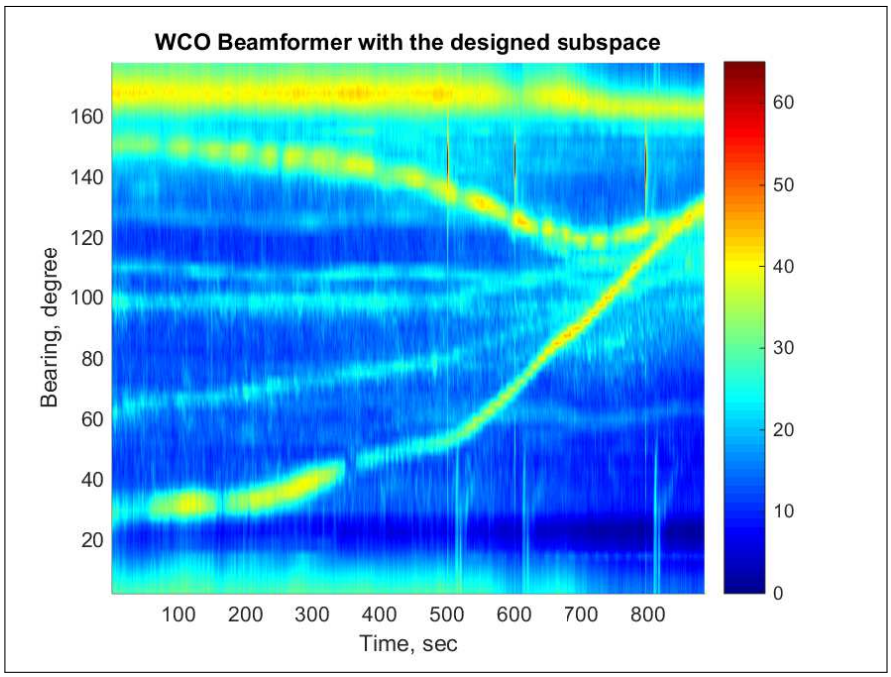

Figure 3.32: Bearing Time Record, Reduced Dimension WCO with ship noise suppression subspace

In order to examine the performance of methods in detail, the detection outputs of the beamformers are presented. For background estimation, two pass split window given in [20] and a constant threshold are used. The constant threshold is intentionally selected a high value to observe the advantage of the designed subspace near the known interference, that is the main ship noise, to other methods tested.

The detection results that are generated by using the same background estimator and the constant threshold are given in the following order

- Detection results of Conventional Beamformer in Figure 3.33,
- Detection results of SMI Beamformer in Figure 3.34,
- Detection results of Worst-Case Performance Optimization Beamformer in Figure 3.35,
- Detection results of Reduced Dimension Worst-Case Performance Optimization Beamformer with the conventional subspace in Figure 3.36,
- Detection results of Reduced Dimension Worst-Case Performance Optimization Beamformer with the designed (nulled) subspace in Figure 3.37.

From the detection outputs of beamformers, the following results are obtained

- With the Conventional Beamformer, the source near the main ship noise and even the main ship noise could not be detected.
- The SMI Beamformer has better performance compared to the Conventional Beamformer but worse than the full dimension WCO beamformer. The main ship noise could not be detected in few instants and the source near the main ship noise could not be detected until approximately 20° difference between the source and the main ship provided.
- The Worst-Case Performance Optimization Beamformer has the best performance among the full dimension methods tested. However, the source near the main ship noise also could not be detected until difference between the source and the main ship increases.

- Reduced Dimension Worst-Case Performance Optimization Beamformer with the conventional subspace performs nearly as good as the full dimension WCO beamformer.

- Reduced Dimension Worst-Case Performance Optimization Beamformer with the designed (nulled) subspace performs as good as the full dimension WCO beamformer. Furthermore, the source near the main ship noise is detected completely. This shows that the suppression of the known interferences while reducing dimension increases the performance of the reduced dimension robust beamformer.

As a result, the performance of the full dimension WCO beamformer is nearly achieved by using the reduced dimension WCO beamformers. Moreover, the performance of the reduced dimension beamformer is enhanced by using the designed subspace that provides suppression of the known interferences while reducing the dimension. Thus, the reduced dimension robust WCO beamformer with a lower computational complexity is obtained.

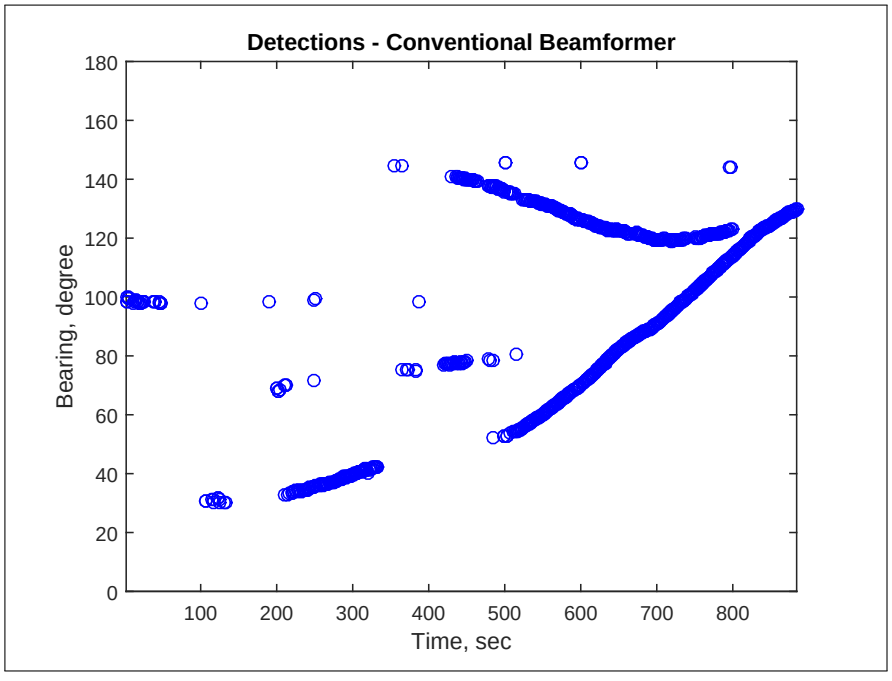

Figure 3.33: Detection outputs of Conventional Beamformer

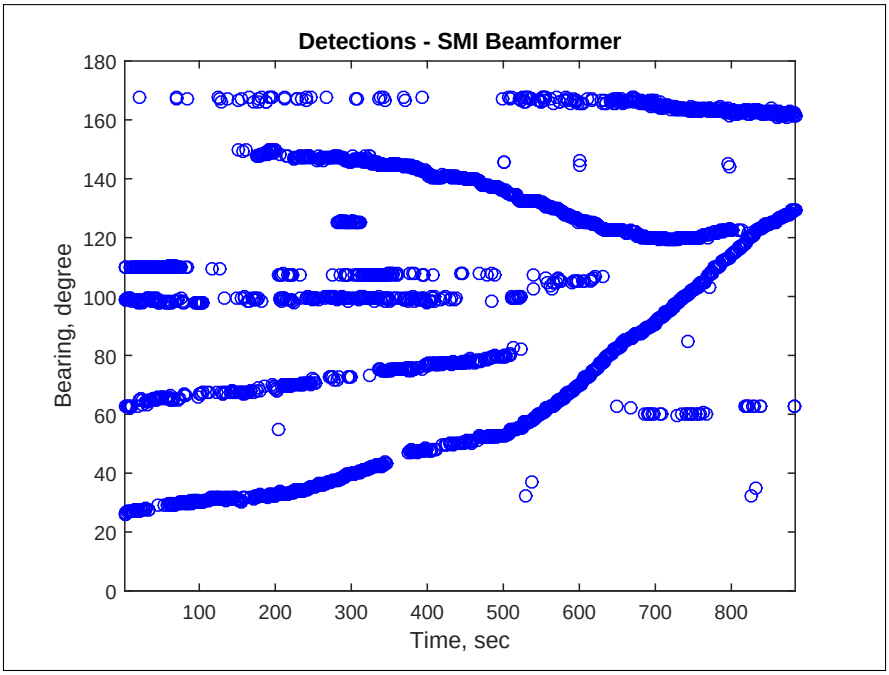

Figure 3.34: Detection outputs of SMI Beamformer

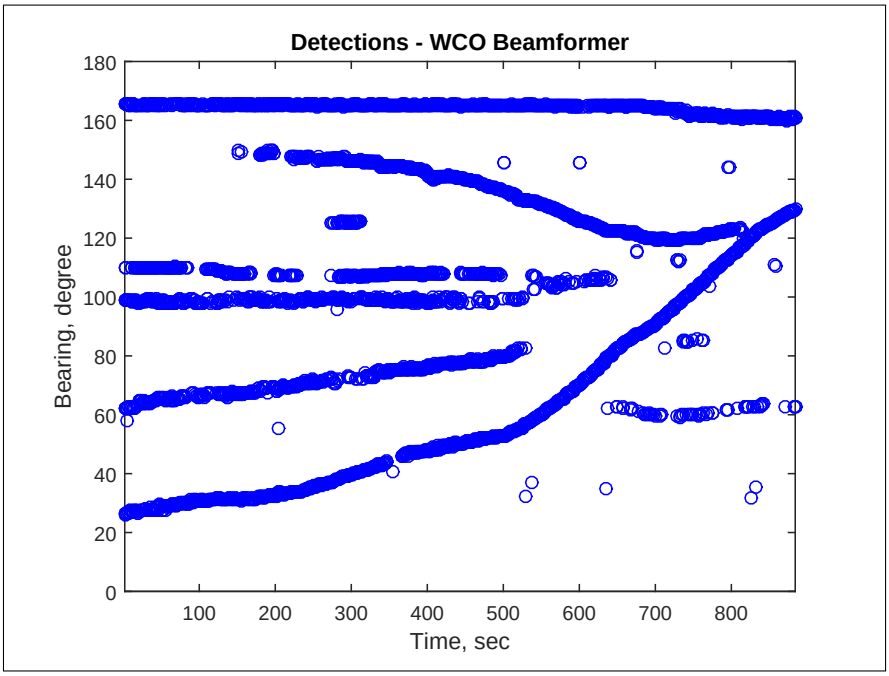

Figure 3.35: Detection outputs of WCO Beamformer

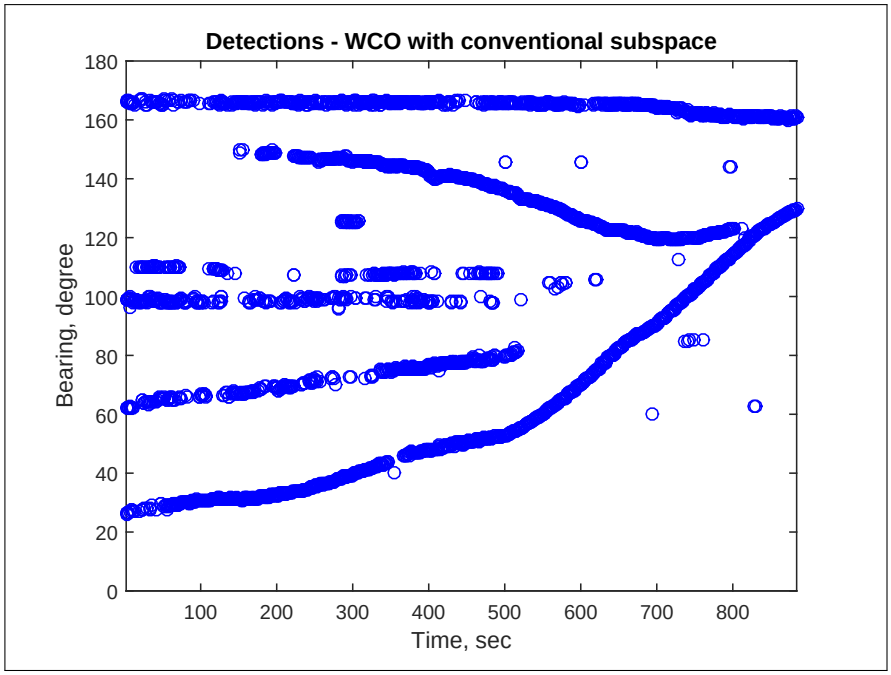

Figure 3.36: Detection outputs of Reduced Dimension WCO with conventional subspace

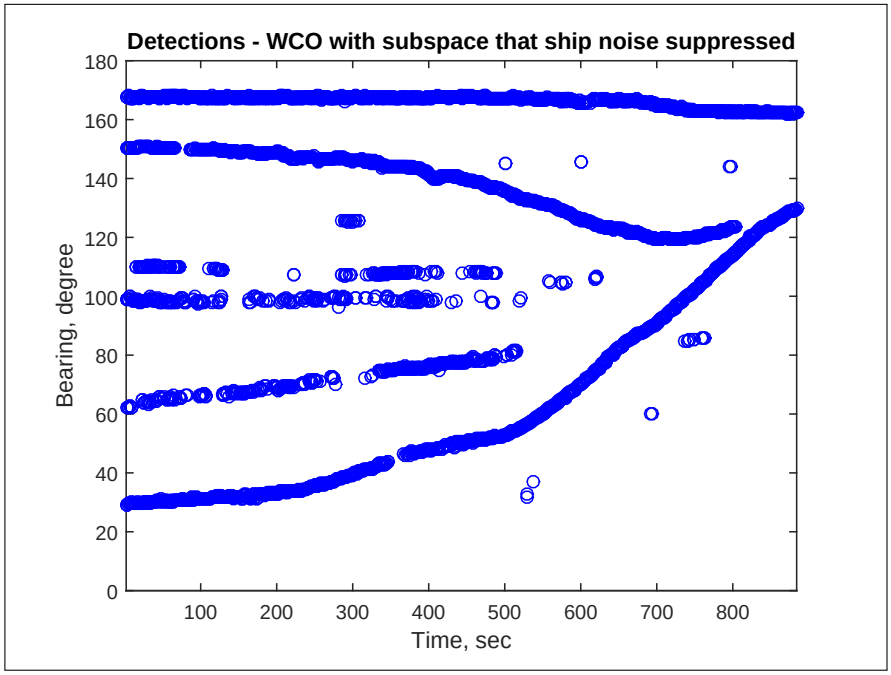

Figure 3.37: Detection outputs of Reduced Dimension WCO with ship noise suppression subspace

CHAPTER 4

DISCUSSION AND CONCLUSIONS

In this thesis, the dimension reduction method used in [23] is applied to the robust adaptive beamforming using Worst-Case performance optimization given in [11] in order to produce quickly converging beamformer allowing for steering vector mismatches and small number of training snapshots. To enhance the performance of this new reduced dimension beamformer, also the special subspace that suppresses the known interferences is developed. For towed arrays, the performance of the developed technique is examined and compared with the full dimension methods.

In Chapter 1, the relevant literature is presented. The data independent beamformer which is the Conventional beamformer, the statistically optimum beamformer also called as MVDR, and the Sample Matrix Inversion are reviewed in Chapter 2. Moreover, the Worst-Case Performance Optimization Beamformer and the reduced dimension implementation of this method are given. Lastly, the subspace design to suppress the known interferences are presented in Chapter 2.

Chapter 3 contains both the simulation and the experimental results. The simulations compare the performance of the methods for five different cases. In the first case, the case of no mismatch in steering vector along with a small number of training snapshots is considered. In this case, firstly the system parameters of the robust methods are determined and utilized in the rest of cases. It is observed that the reduced dimension WCO beamformer with the main-ship noise suppressed subspace has better performance compared as compared with other methods tested in snapshot deficient scenario. Moreover, the conventional

subspace causes fluctuations in the output SINR at the angles near the strong interference if the dimension that the array output is projected is small.

In the second case, the signal look direction mismatch with a small number of training snapshots is considered. The reduced dimension WCO beamformer with the main-ship noise suppressed subspace has also better performance than others; although all methods tested have some performance degradation. Furthermore, it is shown that the SINR performance in this case can be improved by choosing a proper robustness parameter.

In the next case, the sensor placement error with a small number of training snapshots is examined. In this case, it is observed that the full dimension WCO beamformer performs better than the dimension reduced methods since the subspaces used to reduce dimension also comprises the sensor placement error. However, reduced methods still have much higher performance compared to the SMI beamformer.

In the final simulations, the performance of the methods under the coherent and incoherent local scatters with a deficient snapshots is compared. For both cases, a better performance can be obtained by using the dimension reduced WCO beamformer with the main-ship noise suppressed subspace instead of the other techniques.

In the experimental results with the field data, the Bearing Time Records are given for all methods described in Chapter 2 by using the towed array data obtained in sea trials of ASELSAN. Moreover, the detection outputs generated by a generic detector are presented. From presented results, it can be concluded that the Conventional Beamformer has drastically poor performance. The SMI beamformer has weaker output power than the full dimension WCO beamformer due to the mismatches in the assumed steering vector and the small number of snapshot. The dimension reduced beamformers tested have the performance as good as the full dimension robust beamformer. Moreover, the performance enhancement of reduced method with the main ship noise is suppressed subspace is seen from the detection of the source near the main ship noise.

As a summary, a dimension reduced robust beamformer is given by formulating a robust beamforming method in the literature in the reduced dimension. The performance of this method is enhanced by designing a special dimension reducing matrix that suppresses the known interfering sources during reducing dimension. Also, the success of this method is verified with both simulation and experimental results. Thus, a low computational complexity beamformer that is robust against the steering vector mismatch at a low number training snapshots is presented.

REFERENCES

[1] D. Asztely and B. Ottersten. The effects of local scattering on direction of arrival estimation with music and esprit. In *1998. Proceedings of the 1998 IEEE International Conference on Acoustics, Speech and Signal Processing*, volume 6, pages 3333–3336 vol.6, May 1998.

[2] A. Baggeroer and H. Cox. Passive sonar limits upon nulling multiple moving ships with large aperture arrays. In *1999. Conference Record of the Thirty-Third Asilomar Conference on Signals, Systems, and Computers*, volume 1, pages 103–108 vol.1, Oct 1999.

[3] K. Bell, Y. Ephraim, and H. Van Trees. A bayesian approach to robust adaptive beamforming. *IEEE Transactions on Signal Processing*, 48(2):386–398, Feb 2000.

[4] B. Carlson. Covariance matrix estimation errors and diagonal loading in adaptive arrays. *IEEE Transactions on Aerospace and Electronic Systems*, 24(4):397–401, Jul 1988.

[5] L. Chang and C.-C. Yeh. Performance of dmi and eigenspace-based beamformers. *IEEE Transactions on Antennas and Propagation*, 40(11):1336–1347, Nov 1992.

[6] H. Cox. Resolving power and sensitivity to mismatch of optimum array processors. *The Journal of the Acoustical Society of America*, 54(3):771–785, 1973.

[7] H. Cox, R. Zeskind, and M. Owen. Robust adaptive beamforming. *IEEE Transactions on Acoustics, Speech and Signal Processing*, 35(10):1365–1376, Oct 1987.

[8] Y. Doisy, L. Deruaz, and R. Been. Interference suppression of subarray adaptive beamforming in presence of sensor dispersions. *IEEE Transactions on Signal Processing*, 58(8):4195–4212, Aug 2010.

[9] D. Feldman and L. Griffiths. A projection approach for robust adaptive beamforming. *IEEE Transactions on Signal Processing*, 42(4):867–876, Apr 1994.

[10] I. Frost, O.L. An algorithm for linearly constrained adaptive array processing. *Proceedings of the IEEE*, 60(8):926–935, Aug 1972.

[11] A. B. Gershman, Z. quan Luo, S. Shahbazpanahi, and S. A. Vorobyov. Robust adaptive beamforming using worst-case performance optimization: A solution to the signal mismatch problem. *IEEE Trans. Signal Process*, pages 313–324, 2003.

[12] D. A. Gray. Formulation of the maximum signal-to-noise ratio array processor in beam space. *The Journal of the Acoustical Society of America*, 72(4):1195–1201, 1982.

[13] A. Hassanien, S. Elkader, A. Gershman, and K. M. Wong. Convex optimization based beam-space preprocessing with improved robustness against out-of-sector sources. *IEEE Transactions on Signal Processing*, 54(5):1587–1595, May 2006.

[14] A. Hassanien and S. Vorobyov. A robust adaptive dimension reduction technique with application to array processing. *IEEE Signal Processing Letters*, 16(1):22–25, Jan 2009.

[15] Y. Hong, C.-C. Yeh, and D. Ucci. The effect of a finite-distance signal source on a far-field steering applebaum array-two dimensional array case. *IEEE Transactions on Antennas and Propagation*, 36(4):468–475, Apr 1988.

[16] Y. Hua, A. B. Gershman, and Q. Cheng, editors. *High-resolution and robust signal processing*. Signal processing and communications. Marcel Dekker, New York, 2004.

[17] N. Jablon. Adaptive beamforming with the generalized sidelobe canceller in the presence of array imperfections. *IEEE Transactions on Antennas and Propagation*, 34(8):996–1012, Aug 1986.

[18] J. Kim and C. Un. An adaptive array robust to beam pointing error. *IEEE Transactions on Signal Processing*, 40(6):1582–1584, Jun 1992.

[19] J. Li, P. Stoica, and Z. Wang. On robust capon beamforming and diagonal loading. *IEEE Transactions on Signal Processing*, 51(7):1702–1715, July 2003.

[20] R. O. Nielsen. *Sonar Signal Processing*. Artech House, Inc., Norwood, MA, USA, 1991.

[21] I. Reed, J. Mallett, and L. Brennan. Rapid convergence rate in adaptive arrays. *IEEE Transactions on Aerospace and Electronic Systems*, AES-10(6):853–863, Nov 1974.

[22] J. Ringelstein, A. Gershman, and J. F. Böhme. Direction finding in random inhomogeneous media in the presence of multiplicative noise. *Signal Processing Letters, IEEE*, 7(10):269–272, Oct 2000.

[23] S. Somasundaram. Reduced dimension robust capon beamforming for large aperture passive sonar arrays. *Radar, Sonar Navigation, IET*, 5(7):707–715, August 2011.

[24] H. Song, W. Kuperman, W. Hodgkiss, P. Gerstoft, and J. S. Kim. Null broadening with snapshot-deficient covariance matrices in passive sonar. *IEEE Journal of Oceanic Engineering*, 28(2):250–261, April 2003.

[25] P. Stoica and J. Li. *Robust Adaptive Beamforming*. Wiley, Newark, NJ, 2005.

[26] P. Stoica, Z. Wang, and J. Li. Robust capon beamforming. *Signal Processing Letters, IEEE*, 10(6):172–175, June 2003.

[27] H. L. Van Trees. *Detection, estimation, and modulation theory. Part IV. , Optimum array processing*. Wiley-Interscience, New York, 2002.

[28] A. Vural. Effects of perturbations on the performance of optimum/adaptive arrays. *IEEE Transactions on Aerospace and Electronic Systems*, AES-15(1):76–87, Jan 1979.

[29] C. Zahm. Effects of errors in the direction of incidence on the performance of an adaptive array. *Proceedings of the IEEE*, 60(8):1008–1009, Aug 1972.